Construction and Building Materials 450 (2024) 138511

Contents lists available at ScienceDirect

Construction and Building Materials

journal homepage: www.elsevier.com/locate/conbuildmat

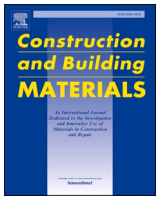

Concrete carbonation in tropical urban and urban/marine environments after 20 years of natural exposure

A.A. Torres-Acosta [a,*], P. Castro-Borges [b], O. Troconis de Rincón [c], B. Martín-Pérez [d], W. Martínez-Molina [e], E. Alonso-Guzmán [e], C. Bernabé-Reyes [e], T. Pérez-López [f], C. Arista-Perrusquía [a], S.E. Crespo-Sánchez [a], J.T. Pérez-Quiroz [g], A. López-Miguel [g], E. López-Vazquez [h], C.E. Juárez-Cruz [i], J.A. Rodríguez [i], F.J. Rodríguez-Gómez [j], M.A. Baltazar-Zamora [k], L. Landa-Ruiz [k], E. Maldonado-Bandala [k], D. Nieves-Mendoza [k], J.A. Moreno-Herrera [l]

[a] Tecnológico de Monterrey, Escuela de Ingeniería y Ciencias, Departamento de Tecnologías Sostenibles y Civil, Epigmenio Gonzales 500, Col. San Pablo, Santiago de Querétaro, Qro. 76130, Mexico
[b] Centro de Investigaciones y de Estudios Avanzados, IPN, Unidad Mérida, Km 6, Carretera Antigua a Progreso, Mérida, Yucatán 97310, Mexico
[c] Universidad del Zulia, Facultad de Ingeniería, Maracaibo, Venezuela
[d] Department of Civil Engineering, University of Ottawa, 161 Louis Pasteur, Ottawa, ON K1N 6N5, Canada
[e] Facultad de Ingeniería, Universidad Michoacana de San Nicolás de Hidalgo, Edificio F, Ciudad Universitaria, Morelia, Michoacán, Mexico
[f] Centro de Investigación en Corrosión, Universidad Autónoma de Campeche, Avenida Agustín Melgar S/N. Col. Buenavista, Campeche, Campeche 24030, Mexico
[g] Instituto Mexicano del Transporte, Coordinación de Ingeniería Vehicular e Integridad Estructural, Km 12+000 Carretera Querétaro-Galindo, Sanfandila, Querétaro 76760, Mexico
[h] Instituto Tecnológico Regional de Oaxaca, Departamento de Ingeniería Civil, Oaxaca, Oaxaca, Mexico
[i] Cementos Holcim, Centro de Innovación Tecnológica para la ConstrucciónToluca, Estado de México, Mexico
[j] Universidad Nacional Autónoma de México, Facultad de Química, Ciudad de México, Mexico
[k] Universidad Veracruzana, Facultad de Ingeniería, Jalapa, Veracruz, Mexico
[l] Facultad de Ingeniería, Universidad Autónoma de Yucatán, Av. Industrias No-Contaminantes por Anillo Periférico Norte, Cordemex, Mérida, Yucatán, Mexico

A R T I C L E I N F O

Keywords:
Carbonation
Corrosion
Concrete
Durability
DURACON

A B S T R A C T

This work is part of the DURACON project, which seeks to characterize the durability of concrete exposed to environmental conditions prevailing in Ibero-America and is based on the exposure of unreinforced and reinforced concrete specimens in marine and urban environments in each participating Ibero-American country. This research presents the results obtained from exposing unreinforced and steel-reinforced concrete specimens to prevailing environmental conditions in twelve natural exposure sites in Mexico during an exposure period of approximately 20 years to determine an empirical model that allows predicting the value of the carbonation rate, k'_{CO2}, as a function of the nth-root of time (NRT) for the concretes evaluated. The concrete specimens, plain and reinforced, exposed to the elements in these cities were manufactured with two types of concrete, one with a w/c ratio = 0.65 and the other with a w/c ratio = 0.45. The tests mainly focused on measuring the concrete carbonation front depth during the ~ 20 years of exposure and the measurement of environmental parameters at the exposure sites, such as temperature, relative humidity, rainfall, and atmospheric CO_2 concentration. The electrochemical parameters of the reinforcing steel (half-cell potential, Ecorr, and current density, icorr) in the reinforced specimens were also obtained after ~ 20 years of exposure to corroborate which sites showed lower or higher corrosion activity. This model to obtain k'_{CO2} as a function of the environmental parameters of the Mexican exposure sites and the physical properties of the concretes was compared with the value of k_{CO2} obtained from the square root of time (SRT) model. It was found that the k'_{CO2} values were 30 % higher on average than the k_{CO2} obtained with the empirical SRT equation. However, it should be noted that k'_{CO2} must be linked to the corresponding n^{th}-root of time, whereas the value of n to obtain k_{CO2} is constant and equal to ½. An agreement was also obtained between the probability of activation of the reinforcing steel, using the corrosion parameters (E_{corr} and icorr), and the probability of $e_{CO2} \leq 15$ mm (lowest concrete cover used in this study).

* Correspondence to: Tecnologico de Monterrey, School of Engineering and Science
E-mail address: atorresa@tec.mx (A.A. Torres-Acosta).

https://doi.org/10.1016/j.conbuildmat.2024.138511
Received 21 March 2024; Received in revised form 23 September 2024; Accepted 24 September 2024
Available online 4 October 2024

1. Introduction

Corrosion of reinforcing steel is one of the most common causes of reinforced concrete structures deterioration, leading to high repair and maintenance costs, along with the concern that this entails for the administrations that are the owners of public works and the individuals whose homes suffer premature deterioration.

Research on reinforcing steel corrosion has been extensive in the last forty years, but it has been primarily focused on 1) the study of the causes and mechanisms of deterioration, 2) the development of electrochemical evaluation and control techniques (both in the laboratory and in situ), and 3) the use of protection methods against deterioration caused by corrosion [1,2]. More recently, the need to quantify the service life of structures affected by corrosion has been raised, so in recent years, the focus has been on the development of models that predict the remaining life of structures in service, or that estimate the future service life in the case of the design of new structures, influencing the project phase [3–5].

The physical characteristics of the concrete cover for the reinforcing steel are related to the structure of the pore network, which is generated due to the excess water that is necessary to use in concrete mixing to make it sufficiently workable. The total porosity of concrete is made up of both closed or occluded pores and a network of pores, whose sizes range from a few μm between < 0.5 nm – 10 nm (gel pores), between 10 nm and 10 μm (capillary pores), up to the order of mm, which are the so-called air pores or large pores [6]. All those that are interconnected are related to the concept of permeability or penetrability, which is the fundamental characteristic that controls the arrival of aggressive agents to the reinforcing steel bar. The permeability of concrete of a specific substance does not depend only on the size and number of pores, as in the case of inert porous materials, but is also influenced by absorption phenomena, the chemical reactions that can occur, the necessary balance of electrical charges during these chemical reactions, etc. [6].

When the ambient humidity is sufficient, these concrete pores are filled with an aqueous liquid consisting mainly of OH^- ions (high alkalinity with a pH between 12 and 13.5), Ca^{2+}, Na^+, K^+ and SO_4^{2-} [1,2,7]. The relative amount of each of them basically depends on the type and proportion of cement used and the water/cement ratio. Furthermore, this composition varies with the age of the concrete, having been shown that after 28 days of age, the Ca^{2+} ion practically disappears from the solution, which becomes almost entirely made up of NaOH and KOH. At this high alkalinity and with the normal O_2 content in buried or submerged structures, the reinforcing steel is covered with a very adherent, compact, and invisible layer of oxides (passivating) that preserves it indefinitely from any sign of corrosion if the concrete is of good quality, is not cracked and does not change its physical or chemical characteristics due to external aggressions [1,2,7].

When the service conditions change and the concrete is altered, or aggressive substances such as chlorides in marine environments or carbon dioxide or sulphur in urban/industrial environments penetrate through it, reinforcement corrosion is triggered with a triple consequence: a) the steel decreases its section or even completely turns into rust; b) the concrete can crack or disintegrate due to the pressures exerted by the accumulating rust; and, c) the steel-concrete bond decreases or disappears [8].

In urban, urban/industrial, or urban/marine environments, concrete carbonation is a problem that is currently affecting many structures in our countries due to the diversity of climates that exist. Although on a smaller scale than the problem caused by chloride ions, concrete carbonation has more complex conditions for its prediction [4]. This is because it does not only involve a diffusion process, but the chemical reaction between the aggressive agent CO_2 and the cement hydration products in concrete is more significant than with chloride ions. Thus, these problems are directly related to the chemical characteristics of concrete and the weather parameters of the environment to which the structures are exposed [3–5].

Different definitions have been given to the concept of service life concerning the durability of a concrete structure [1,2,7]. From the point of view of reinforcement corrosion, a simple model has been proposed by Torres-Acosta and Martinez-Madrid attempting to define all the parameters that could allow an estimate of the service life or durability of a given structure under service conditions with an adequate structural capacity safety coefficient [9]. Together with the results of the physical-chemical and electrochemical evaluation of the different specimens exposed to natural environments in tropical countries, these models will allow us to define a better way to design durable concrete structures and adequately repair existing ones that exhibit this problem [3–5].

Previous research has investigated concrete carbonation, mainly in controlled environments, most of them under accelerated conditions using special chambers that control humidity and temperature, and inside which, a concentration of CO_2 of 10–100 times more than in a natural environment is added [10]. Results of studies on concrete carbonation in specimens exposed to natural exposure environments have also been presented by the DURACON International Project [4]. This previous investigation correlates the physical/chemical characteristics of the concrete used with the meteorological parameters of the urban and urban/marine exposure sites and with the concrete carbonation depth [4]. The International group also generated a neural network simulation with the data collected from the test sites from all countries involved in the project for the initial 5-year exposure period [11]. However, the information previously presented from the DURACON Project in references [4] and [11] corresponded to an exposure of less than 5 years and 10 years, respectively, so it is necessary to corroborate this information obtained with results from exposures to urban or urban/marine environments at longer exposure periods.

This is the motivation for presenting the results of the DURACON Project for the twelve Mexican sites, which have reached an exposure time of $\sim$ 20 years. Likewise, empirical equations were obtained to determine the most critical parameter in the concrete carbonation phenomenon called carbonation coefficient (k_{CO2}) based on the physical/chemical characteristics of the concrete and the environmental parameters of the twelve sites of the DURACON Project in Mexico.

2. Research significance

There has been an increase on the research groups working on topics related to reinforced concrete durability. Many of the groups have presented short-term ($<$ 2 years) experimental information to reach some results and conclusions on concrete durability that may not be completely certain for long term performance. Also, ambient temperature and humidity in laboratory regularly is controlled, and no rainfall affects the performance of the specimens. Durability performance information obtained from reinforced concrete structures, or structural elements, are scarce because need several years to have interesting information. This investigation presents natural exposure outside controlled environments for a period of $\sim$ 10 years, therefore, different climate exposure is analyzed based on the experimental results observed during this period of time, which in turn is the most important contribution of the present investigation.

3. Methodology

3.1. Materials

All concrete specimens were manufactured with Portland cement type I (corresponding to a CPO according to Mexican cement nomenclature [12]). Table 1 shows the physical/chemical characteristics of the

cement used to manufacture the concrete in this research. With this information, the clinker phases were estimated using Bogue calculation [6], resulting in the following percentage contents: C_3S of 54.0; C_2S of 20.5; C_3A of 13.8; and C_4AF of 3.5.

Two water/cement (w/c) ratios of 0.45 and 0.65 were specified in the concrete used to manufacture the specimens to be exposed in the natural exposure sites. The aggregates used for the manufacture of concrete were silica sand as fine aggregate (with a fineness modulus < 3) and gravel as coarse aggregate (with a maximum aggregate size of 13 mm). Both aggregates met the grading limits established by ASTM C-136 [13]. Table 2 shows the proportions for both types of manufactured concrete.

A total of 12 prismatic concrete specimens measuring 15x15x30 cm were manufactured for each of the test sites. Six of the specimens were plain concrete without reinforcement, and six were reinforced with reinforcing steel. Six reinforcing steel bars of 10 mm in diameter were used in the reinforced concrete specimens, with concrete covers of 15, 20, and 30 mm for each pair. Fig. 1 illustrates the arrangement of the reinforcing bars in each of the prisms. For example, Fig. 2 shows the exposed prisms at the sites in Queretaro (QRO), Morelia (MOR), Mexico City (CDMX), and Toluca (TOL), Mexico. Fig. 3 shows a map of Mexico with the locations of the fifteen exposure sites that were initially set up for the DURACON Mexico project. This investigation presents results of only twelve test sites, from the original fifteen test sites initially.

The concretes were characterized after 28 or 90 days of curing in a curing chamber at a temperature of 22±2℃ and a controlled humidity >95 %. The mechanical characterization of these concretes included: 1) the compressive strength using the standardized ASTM CC-39 procedure at 28 and 90 days curing (the cylinders were kept saturated until the test date) [14]; 2) indirect tensile strength at 28 days curing using the standardized procedure of ASTM C-496 [15]; and, 3) the elastic modulus at 28 days curing using the standardized method ASTM C-469 [16]. The physical characterization consisted of obtaining the transport properties of the concrete at ages older than 90 days and included the following: 1) total absorption using the standardized method ASTM C-642 [17]; 2) total porosity using the ASTM C-642 method [16]; 3) effective porosity, using the method described by Fagerlund [1,18]; and, 4) saturated electrical resistivity of the concrete, following the standardized procedure of ASTM C-1876 [19].

3.2. Environmental monitoring

To obtain the environmental parameters, the exposure sites were located near meteorological stations run by the institution responsible for the exposure site or near a meteorological station that could provide the ambient data for that specific site. Fig. 4 shows the weather station of the city of Queretaro (QRO), Mexico. The main climatic-environmental parameters that were recorded were the ambient relative humidity (RH), the wind speed (WS), the daily rainfall (RF), the temperature at intervals of 15 minutes (T), and the CO_2 concentration (one measurement per year).

It should be noted that of the fifteen exposure sites initially set up in Mexico, three were in operation for a period between 7 and 10 years, after which the specimens were lost due to reasons unrelated to the project. These sites were those located in Mexicali (MEX, urban), Chihuahua (CHI, urban), and Tampico (TAM, urban/marine). This is why the information collected (meteorological data, concrete carbonation front depth, and electrochemical measurements of the reinforcement) was only obtained between years one and five.

Table 2
Concrete mixture proportions.

MIXTURE	Proportions (kg/m^3)				
	Cement	Water	Coarse	Sand	Additive*
w/c: 0.65	285	185	1033	812	2
w/c: 0.45	411	185	1010	731	4

* Water reducer

3.3. Tests to determine the depth of carbonation

The unreinforced concrete specimens were cut into slices using a special guillotine-type machine designed to make transversal cuts to the prismatic concrete specimens. These sections were sprayed with a pH indicator solution based on phenolphthalein, alcohol, and distilled water in a proportion of 1 g: 850 ml: 150 ml [1–4,7,10]. The depths from the external surface of the specimen to the boundary of color change were measured at a minimum of four different points on each edge of the square perimeter of the cut slice. The carbonation depth was estimated as the average value of the measurements from the four faces of the three specimens of each type of concrete.

3.4. Physical/chemical characterization of concrete

Once the carbonation depth measurements were completed, the slices were cut to proceed with the physical/chemical evaluation of the concrete after the exposure time and to determine the possible changes that the concrete might have undergone due to the exposure environment (Fig. 5). The cuts for each slice's physical/chemical characterization depended on whether the slices evaluated came from an urban or urban/marine site.

The cuts of the slices obtained from the urban site specimens are shown in Figs. 5a and 5b for the concrete with a w/c ratio of 0.45 and 0.65, respectively. The cuts of the slices obtained from the urban/marine site specimens are shown in Figs. 5c and 5d for the concrete with a w/c ratio of 0.45 and 0.65, respectively. These cuts were defined based on the physical/chemical information to be collected in each of the cuts made.

Since the concretes with a w/c ratio of 0.45 did not have a significant carbonation depth after ~20 years of exposure, the slices from the urban sites were divided in such a way to obtain cuts with a cube (cuts 2–1, 2–2, and 2–3) and a prismatic (cuts 1 and 3) geometry to determine the saturated electrical resistivity (ρ_S) of the concrete (Fig. 5a). The average ρ_S of the slice was determined as the average of the values obtained from the five cut specimens.

The concretes with a w/c ratio of 0.65 did present considerable carbonation after ~20 years of exposure, so the slice cuts were made to obtain concrete samples without carbonation (cuts 2–2, 3–2, 3–3, 3–4, and 4–2) and with carbonated concrete (cuts 1, 2–1, 2–3, 3–1, 3–5, 4–1, 4–3, and 5). In this way, the measurements of ρ_S could be differentiated depending on whether the concrete was carbonated (Fig. 5b).

For the slices of the specimens from the urban/marine sites, the cutting diagrams were different from those made in the slices from the urban sites, giving greater importance to the penetration of chlorides rather than to the ρ_S of the concrete. More samples were thus cut from these slices to obtain a more detailed chloride penetration profile

Table 1
Physical/chemical characterization of Portland cement type CPO.

SiO_2 (%)	Al_2O_3 (%)	Fe_2O_3 (%)	CaO (%)	MgO (%)	Na_2O (%)	K_2O (%)	SO_3 (%)	Total Alkali	Insoluble Residue	Ignition Loss (%)	Free Lime (%)
21,38	4,22	4,54	63,37	1,51	0,16	0,53	2,32	0.51	0.54	2.92	0.66

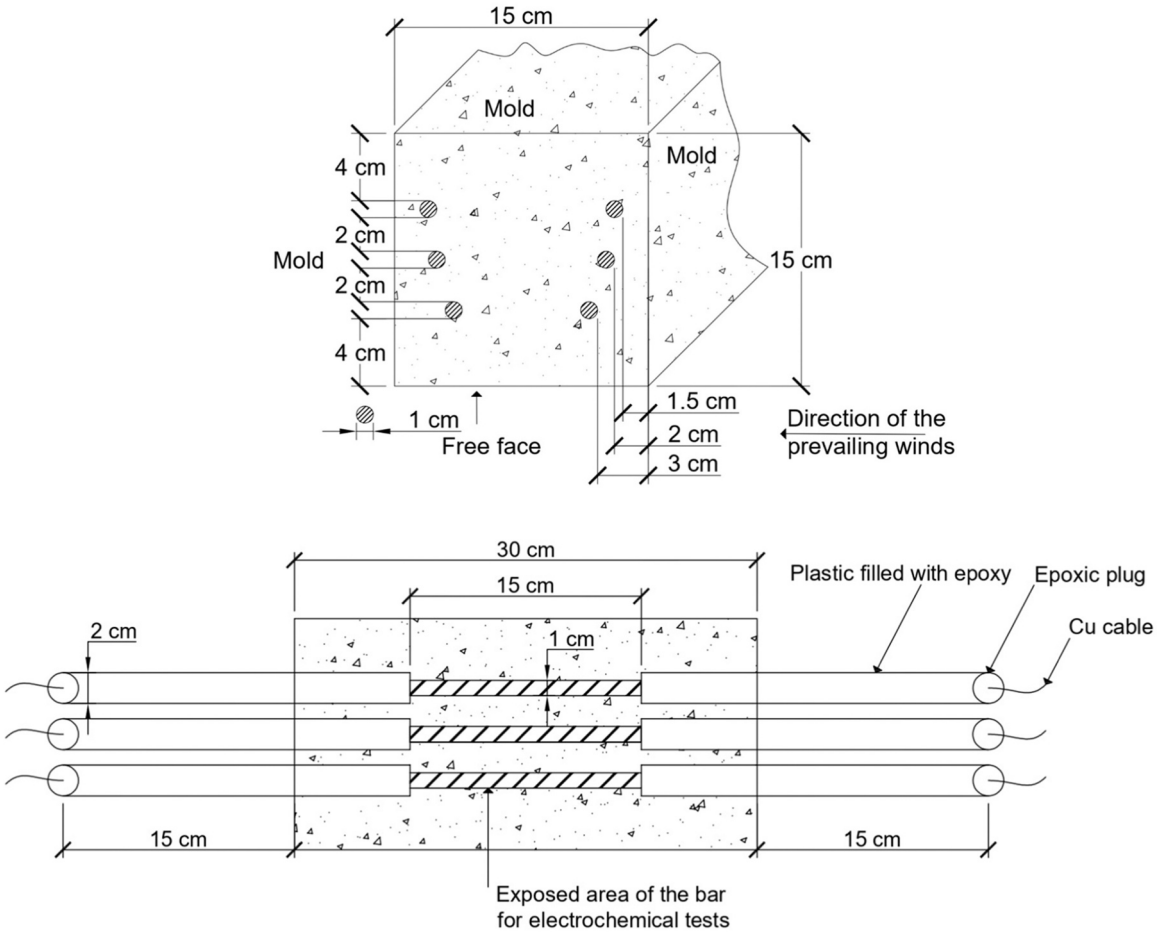

Fig. 1. Geometric details of reinforced concrete prismatic specimen.

Fig. 2. Monitoring sites in (a) Queretaro (QRO) Mexico; (b) Morelia (MOR) Mexico; (c) Mexico City (CDMX); and (d) Toluca (TOL), Mexico.

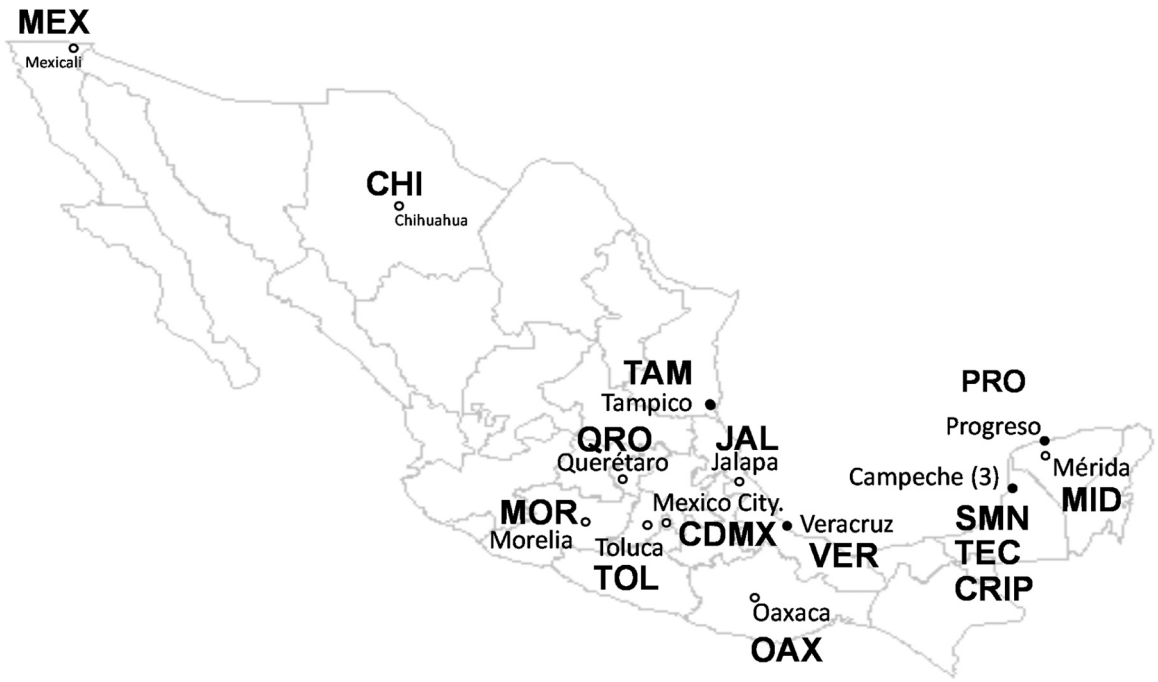

Fig. 3. Natural exposure sites of DURACON-México project: 9 urban sites and 6 urban/marine sites. The urban/marine exposure sites are denoted with a solid black circle.

Fig. 4. Monitoring weather site in the city of Querétaro, Mexico.

(Figs. 5c and 5d). The corner cuts of each slice (cuts 1–1, 1–2, 3–1, 3–2, 2–1, 2–2, 4–1, and 4–2) were used to measure ρ_S.

As already mentioned, the first physical property measured in the concrete of the specimens exposed at the Mexican sites after ~20 years was the ρ_S. Once the concrete samples were cut from the slices, they were weighed to obtain their original mass and then placed in a sealed container with humidity > 90 %. The mass change (due to moisture absorption) and the electrical resistivity in semi-saturation (ρ) were monitored for each concrete sample. The measurement of ρ was carried out by the volumetric method according to ASTM C-1876 [19]. Once the sample had reached a constant mass and ρ (constant mass is defined when the difference between two successive measurements is less than

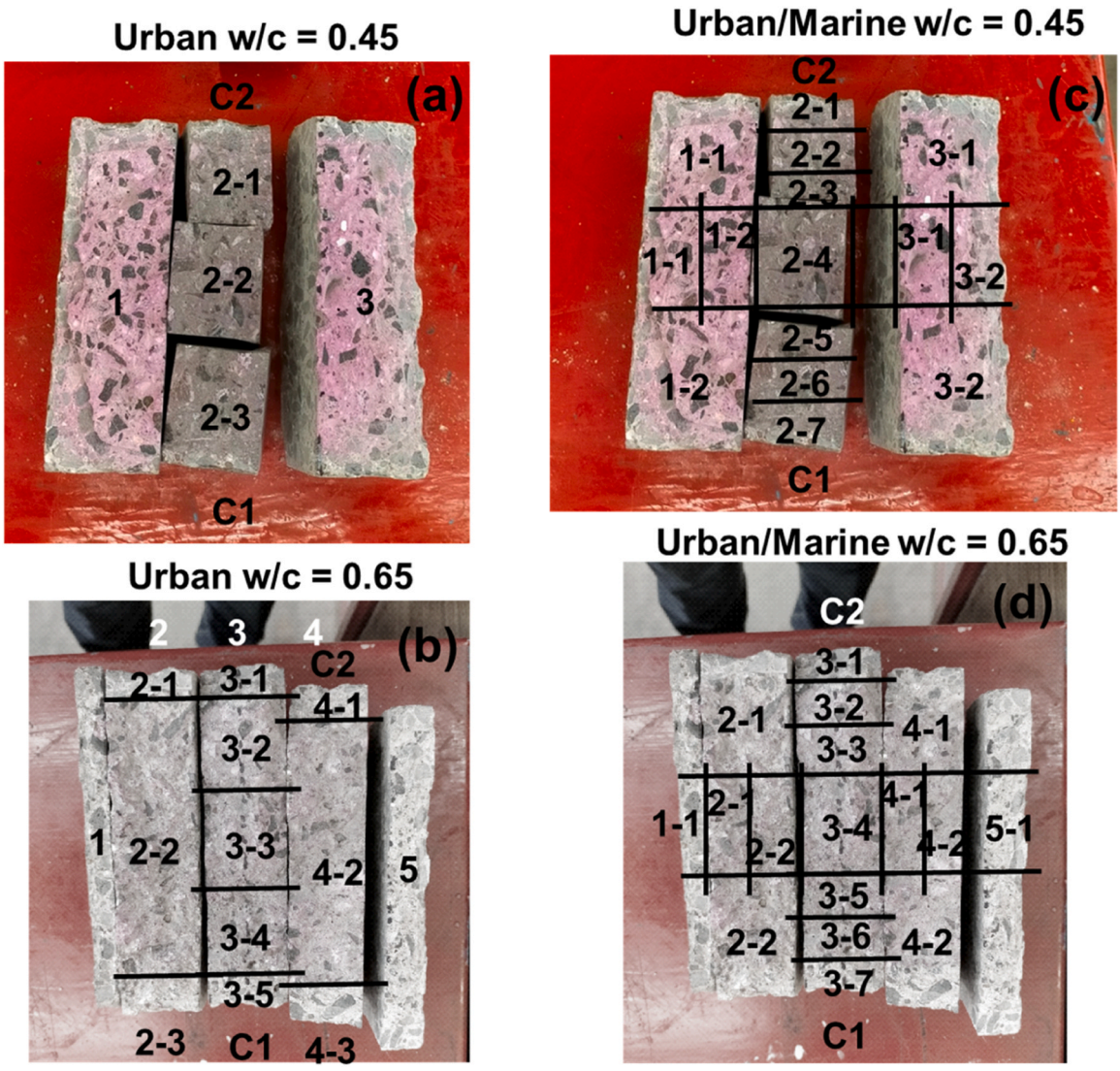

Fig. 5. Slice cuts to obtain samples to determine the physical/chemical properties of the evaluated concretes taken from MOR, Mexico, test site.

0.5 %), the value of ρ was recorded as ρ_S.

The following physical property determined was the percentage of total voids (%TV) using the samples used to determine ρ_S. The standardized procedure in ASTM C-642 [17] was followed to determine % TV, starting with obtaining the saturated mass (m_S), which was the last mass measurement of the procedure to obtain ρ_S. Immediately afterwards, the submerged saturated mass (m_{SS}) was measured with the same sample, using a hydrostatic balance. Once the m_{SS} values were obtained, the specimens were placed inside an oven to dry at a temperature of 50 ±2°C until constant mass. These values are defined as the dry mass (m_D). Once these three mass values (m_S, m_{SS} and m_D) are obtained, the %TV is estimated from:

$$\%TV = 100 \text{ x } (m_S - m_D) / (m_S - m_{SS}) \quad (1)$$

The chemical property obtained from the slices cut from the concrete specimens was the concentration of free (water-soluble) and total (acid-soluble) chlorides, using the other cuts shown in Figs. 5c and 5d (concrete with w/c of 0.45: cuts 1–1, 1–2, 2–1, 2–2, 2–3, 2–4, 2–5, 2–6, 2–7, 3–1, and 3–2; concrete with w/c of 0.65: cuts 1–1, 1–2, 2–1, 2–2, 3–1, 3–2, 3–2, 3–4, 3–5, 3–6, 3–7, 4–1, 4–1, and 5–1). The results of the chemical analyses to determine the chloride profiles in these slices from the urban/marine sites are not part of this investigation and will be presented in a subsequent publication.

3.5. Electrochemical monitoring of reinforcing steel

The reinforcing steel in the reinforced prismatic specimens was used to perform the electrochemical monitoring through the measurement of the half-cell potential (or corrosion potential, E_{corr}) and the corrosion current density (i_{corr}) using the procedures in references [1,7,20] and [1, 7], respectively. The equipment used to carry out these measurements was field equipment that used the guard ring technique to confine the signal to obtain a result as accurately as possible [1,7]. At the beginning of the project, this monitoring was carried out with a frequency of 1–4 months, obtaining between 3 and 12 electrochemical measurements per year. The last measurements were carried out after ~20 years of exposure and are the only results presented herein. The values obtained from the equipment were the corrosion potential (E_{corr}), the current density or corrosion rate (i_{corr}), and the electrical resistance of the concrete (R_S, more specifically, of the specimen concrete cover).

4. Results

4.1. Concrete properties

Table 3 shows the values of the physical/mechanical properties of the concretes manufactured in this study at 28- and 90-day age. As can

be seen in Table 3, the concrete with a w/c ratio of 0.65 had physical properties that correspond to concretes with better performance than those obtained from the so-called conventional concrete since its compressive strength at 28 days of age was above 30 MPa and its total porosity < 16 %.

The physical/mechanical properties of the concrete with a w/c ratio of 0.45 reached higher performance values, as intended when selecting the mix design proportions, to achieve one concrete of superior performance to the conventional one (the one with w/c of 0.65) and another with a relatively high performance (the one with w/c of 0.45).

4.2. Environmental monitoring of exposure sites

Because, in total, there is information from twelve exposure sites for ~20 years, Fig. 6 shows the monitoring of four meteorological variables (wind speed, WS, temperature, T, relative humidity, RH, and rainfall, RF) for only one test site: Toluca. These meteorological measurements, collected every 30 minutes, were averaged daily, and then a monthly average was obtained. These monthly average values are those shown in Fig. 6 for the site mentioned in the respective figure.

4.3. Carbonation depth measurements

Figs. 7 and 8 show the average carbonation depth e_{CO2} measured in the prismatic unreinforced specimens for the concretes with w/c ratio of 0.45 and 0.65, respectively, which were obtained on the slice cutting dates and using the method described with the pH indicator (phenolphthalein); the average values were obtained from three slices with 12–16 measurements per specimen, giving a total of measurements between 36 and 48 per type of concrete and cutting date.

4.4. Physical properties of concrete after ambient exposure

Once the slices were cut to determine the e_{CO2} values for each concrete and each site, the next step was to cut the slices into cubes or prisms of the same material to determine the physical/chemical properties of the concrete after ~20 years of exposure. These physical/chemical properties included the determination of ρ_S, %TV, and the concrete's chloride concentration profiles (the latter's results are not included in the present study).

The values obtained for ρ_S and %TV are shown in Figs. 9 and 10, where the typical results obtained from only two sites (TOL and QRO) are presented as an example since data from all sites would extend the content of this publication if they were all shown, like the photographs of the arrangement of the specimens at the site in Fig. 2 and the meteorological data presented for TOL test sites in Fig. 6.

Using a cumulative statistical curve, the ρ_S and %TV results are presented graphically as a cumulative fraction. This graph is obtained from each measurement obtained on each specimen used for said measurement (cube or prism cut from the slices), ordered from lowest to highest values on the abscissa axis (X-axis). The number of measurements varied from 10 to 15 data points, depending on the number of prisms or cubes obtained from the slices cut on each prism exposed at the sites. For each of these ordered values, the ordinate axis (Y-axis) value is estimated from the order number 1/n, where n is the number of measurements in that set. For example, if the number of %TV values for the Toluca site were 10 for the concrete with a w/c ratio of 0.45, the smallest value of %TV would have a value on the Y axis of 1 /10 = 0.1, the second smallest %TV value would have a Y-axis value of 2/10 = 0.2, and so on.

Table 3
Physical/mechanical properties of concrete.

PROPERTIES		MIXTURE	
		w/c: 0.65	w/c: 0.45
Fresh concrete unit weight (kg/m^3)		2316	2329
Compressive strength (MPa)	28 days	31.0	51.5
	90 days	41.6	67.9
Indirect tensile strength at 28 days (MPa)		1.2	3.6
Modulus of elasticity at 28 days (GPa)		18.1	22.5
Total absorption (%)		7.55	6.3
Total porosity (%)		16.5	14.0
Effective porosity, Fagerlund's method (%)		11.3	8.7
Saturated electrical resistivity at 90 days, ρ_S (kΩ·cm)		23	39
Rapid chloride permeability at 56 days (Coulombs)		1140	710

4.5. Electrochemical measurements on reinforcing steel

Electrochemical measurements were carried out at all sites using the prismatic specimens reinforced with six bars each and the equipment mentioned above. Since much data were collected from the 12 operating test sites, electrochemical measurements are presented using the same type of graph used to represent ρ_S (Fig. 9) and %TV (Fig. 10) in the previous section, called representation diagrams. In this case, the parameters represented are the E_{corr} and i_{corr} of the reinforcing steel and the R_S of the concrete, as illustrated in Fig. 11.

5. Discussion

5.1. Effect of meteorological parameters at exposure sites

The information was collected by those responsible for the monitoring sites or through information from government meteorological stations close to the exposure sites of the concrete specimens. These data were obtained at intervals that could be minutes or hours and analyzed to give average monthly values and, finally, average annual values during the ~20 years of exposure.

The meteorological data were further analyzed to develop empirical models that correlate these values with concrete parameters and concrete carbonation, presented later in this publication. These values were averaged at each site, such that an annual average of the monthly averages was obtained, and the annual average of the meteorological results was averaged for each site. The average values of each site, corresponding to the average of the years in which this meteorological information was captured for each environmental variable, are listed in Table 4. The values of the MEX, CHI, and TAM test sites correspond to the first five operating years of exposure before closing those test sites due to reasons unrelated to the project.

5.2. Effects of natural exposure on concrete carbonation

The experimental e_{CO2} results obtained at the twelve test sites show a marked increase in e_{CO2} after ~20 years of natural exposure in the concrete with a w/c ratio of 0.65. The advancement of the carbonation front in the concrete with a w/c ratio of 0.45 showed a similar increase as the concrete with a w/c ratio of 0.65 in the first 4–5 years of exposure; however, the carbonation front depth e_{CO2} for the concrete with a w/c ratio of 0.45 remained almost constant between the value obtained after 4–5 years of exposure and the value obtained after ~20 years of exposure.

Fig. 8 shows that the e_{CO2} in the concrete with a w/c ratio of 0.65 increases throughout the ~20 years of exposure, with an appreciable decrease in the carbonation rate at the end of the exposure. On the other hand, the carbonation performance of the concrete with a w/c ratio of 0.45 (Fig. 7) was modified once the e_{CO2} value apparently reached a limit depth that prevented CO_2 (gas) from advancing into the concrete, since e_{CO2} between 4 and 5 years and ~ 20 years was almost the same. As it is well known [21,22], concrete carbonation further decreases concrete's permeability, controlling its subsequent carbonation (Figs. 7 and 8), especially in good quality concrete where the capillary porosity is very small. Another important effect observed in the DURACON-Mexico project is the movement of alkalis in some sites,

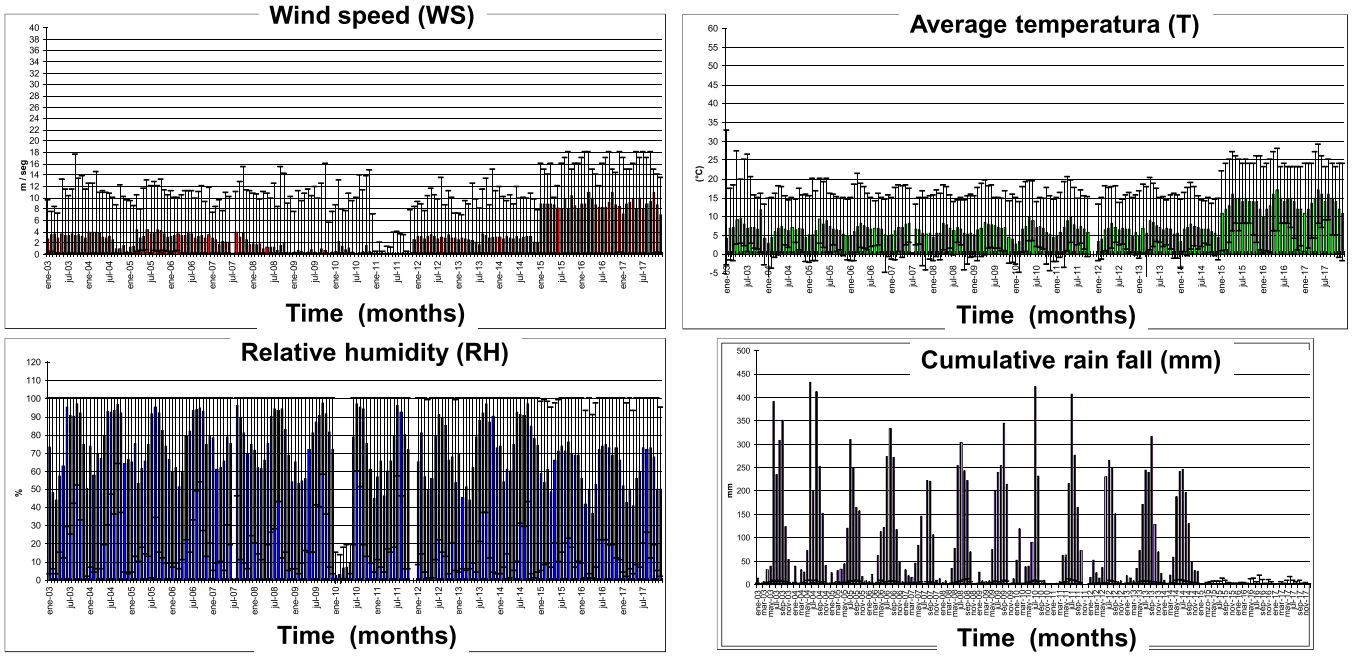

Fig. 6. A sample of meteorological data obtained from the natural exposure site in the city of TOL, Mexico (urban).

mainly $Ca(OH)_2$, towards the carbonated zone, re-alkalinizing part of it and reducing the carbonation depth. The re-alkalinization delays the carbonation front from reaching the reinforcement and thus triggering corrosion when only CO_2 and water are the only environmental hazards. This re-alkalinization performance was only noticed when the concrete specimens were exposed to a natural environment without being protected from environmental changes, mainly rain, relative humidity, and temperature in the exposure locations.

Although there are concrete carbonation studies under normal outdoor exposure conditions [23–30], there have also been many research projects that evaluate concrete carbonation under sheltered locations (inside the laboratory with regularly controlled temperature and humidity), thus avoiding contact of the specimens with a changing environment due to rain, humidity, or temperature cycles. If the experimental program for exposing the specimens, however, uses accelerated carbonation chambers, the interior of these chambers (where the concrete specimens are placed) is maintained at an even more controlled temperature and humidity regime than in a natural exposure inside the laboratory (without accelerating CO_2 exposure). This is why the natural exposure sites selected in this research (most sites were selected in between the tropics, with a higher temperature regime than in septentrional countries in North America, Europe, and some Asian regions) could have generated modifications to the carbonation process in the concrete with a w/c ratio of 0.45, which is the one with the highest cement content and the lowest porosity of the two evaluated concretes, as shown in the concrete properties presented in Table 3.

After observing a constant e_{CO2} between 5 and ~20 years of exposure for the concrete with a w/c ratio of 0.45, it is hypothesized that changes in rainfall, humidity, and temperature on the surface of the concrete specimens may have led to a process of re-alkalinization during the ~20 years of natural exposure. It seems that during this period of long exposure, the CO_2 penetrated the concrete when its porosity had free space for the CO_2 gas to enter and initiate the reaction with the capillary water and the hydrated products of the cement, which are necessary for the chemical reactions of concrete carbonation to occur. Once the concrete was carbonated, the humidity of the environment could have increased at the exposure site, either because solar radiation becomes null at night or because it rains, and the exposed specimens get wet. This would cause the concrete to absorb this excess moisture or water into the specimen, and this moisture could enter to a greater depth than the depth of the already carbonated concrete. When the specimen is saturated inside to a depth greater than the carbonated depth, it can dry out because of solar radiation the next day, for example, and together with an increase in the exposure temperature during midday, the absorbed water can evaporate and move outward bringing alkaline products with it and leading to re-alkalization of the concrete to a certain depth.

This process of cyclic wetting and drying over several years could have generated this phenomenon and, therefore, halted the gradual and constant carbonation process inside the concrete, a situation that is observed after ~20 years of exposure of the specimens in this investigation, where the e_{CO2} values did not change between 5 and ~20 years of exposure. On the other hand, concrete specimens with a w/c ratio of 0.65 did not show this stagnation in e_{CO2} values, and the concrete continued to carbonate with increasing exposure time. This difference in the carbonation of these concretes, compared to those with a w/c ratio of 0.45, could have been because the concretes with a w/c ratio of 0.65 did not have enough alkaline matter inside to generate this re-alkalinization process. In addition, these concretes have a greater porosity that allows the passage of more CO_2 inside the specimens, and thus, the concrete carbonates faster than it can be re-alkalized. This hypothesis must be corroborated in the future by having more experimental information reproducing these wetting-drying cycles and temperature changes; it is expected to have this information soon.

Another distinction observed in Figs. 7 and 8 is the difference in carbonation depth between specimens exposed to urban and urban/marine sites; specimens exposed to urban sites were carbonated more than the ones in the urban/marine sites for both types of concrete. This is why separate graphs were generated for the e_{CO2} values obtained in the urban sites (Figs. 7a and 8a) and the urban/marine sites (Figs. 7b and 8b). This difference is because the concrete specimens in the urban/marine sites have considerable internal chloride contamination, shown in a previous publication wherein the chloride concentrations inside the concrete specimens exposed to these environments were reported [3].

The chlorides inside the concrete make it more hygroscopic, increasing the internal humidity of the specimens. This, coupled with

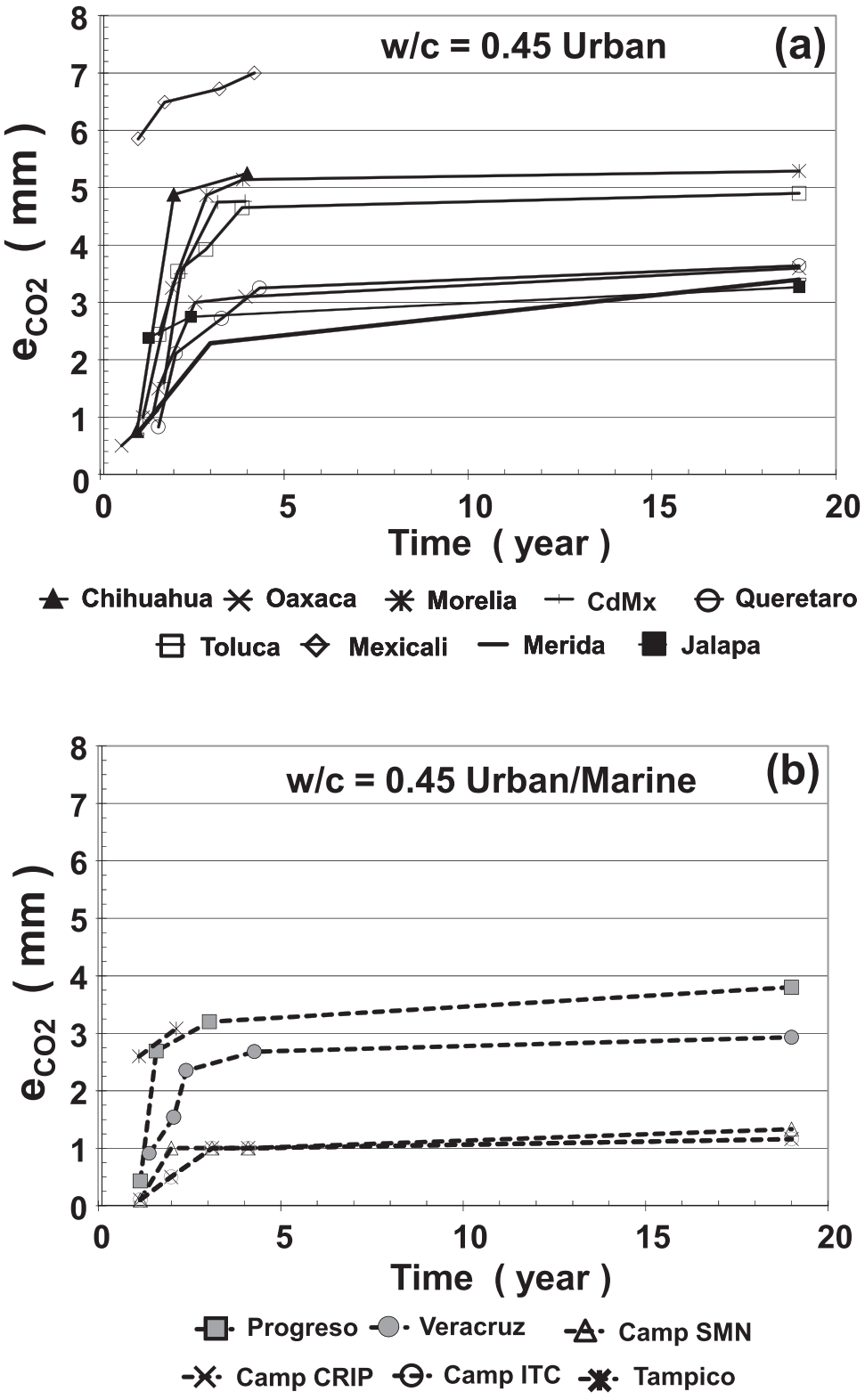

Fig. 7. Carbonation depth (e_{CO2}) of concrete with w/c of 0.45: a) urban sites; (b) urban/marine sites.

the fact that the relative humidity and temperature are higher at these test sites (see Table 4), hinders the entry of CO_2 gas into the interior of the concrete, as its pores are more saturated than those in the concretes exposed to urban sites located in the interior of the country and far from the coast [4,5]. Again, this information must be corroborated with more data obtained from future research.

Another reason that could have slowed down the carbonation reactions in the concrete is the transformation of the cement hydration products into calcium carbonate ($CaCO_3$) in the region of the carbonated material itself. The chemical process of transforming the cement hydration products into $CaCO_3$ decreases the porosity of the concrete since more solids are produced, reducing the empty spaces left as capillary porosity in the carbonated concrete [4]. This phenomenon is observed in Figs. 9 and 10, which show the physical properties ρ_S and %TV measured

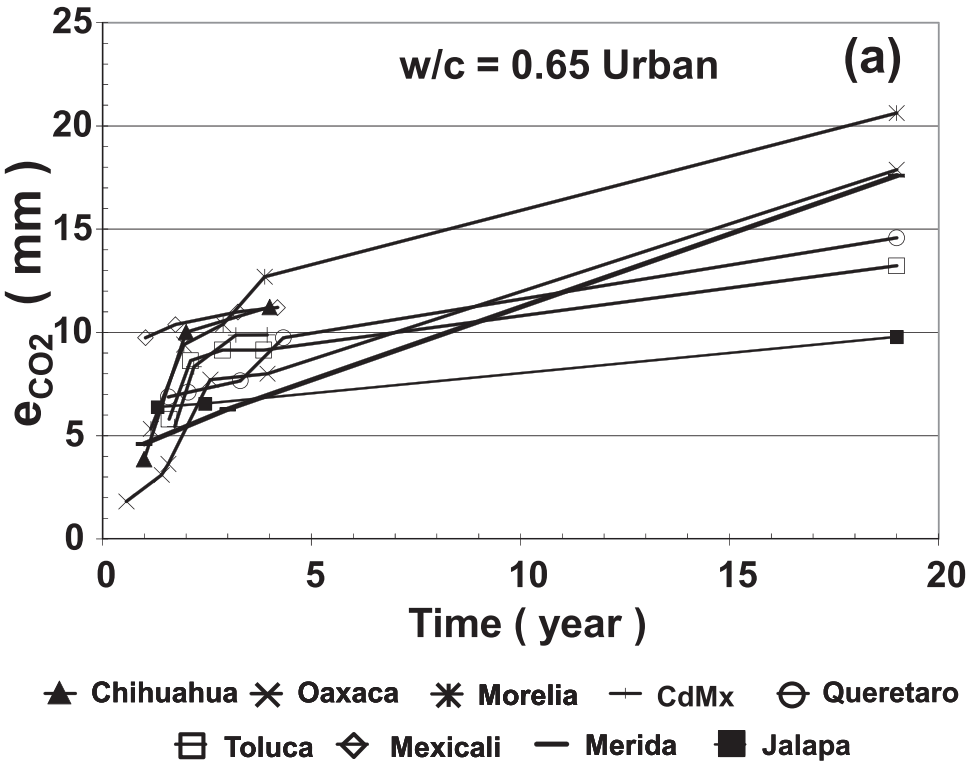

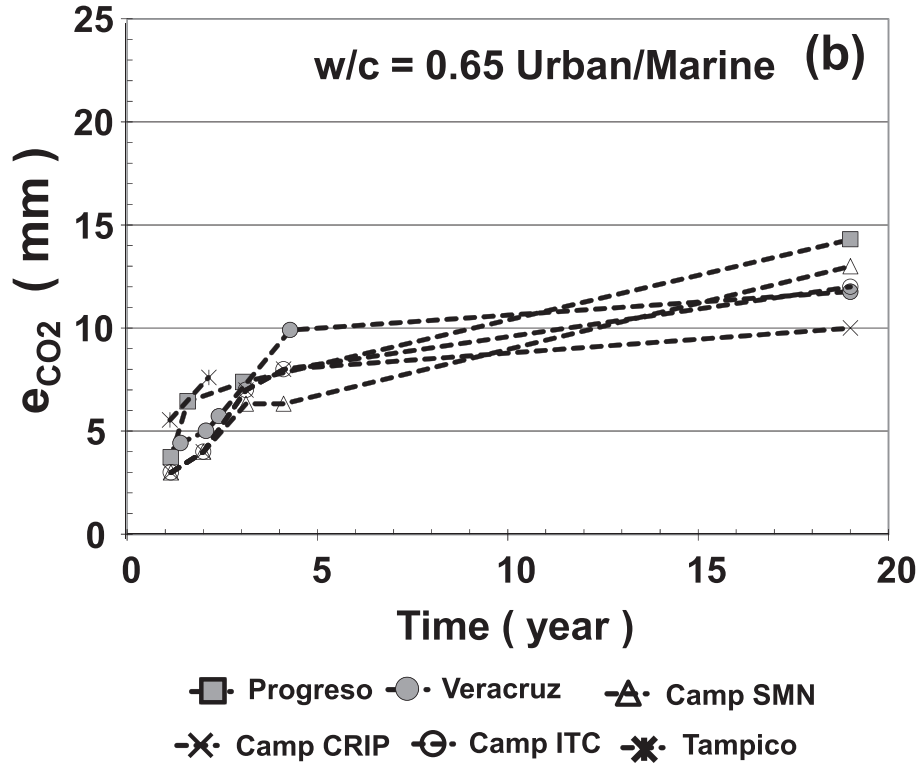

Fig. 8. Carbonation depth (e_{CO2}) of concrete with w/c of 0.65: a) urban sites; (b) urban/marine sites.

in both concretes with a w/c ratio of 0.45 and 0.65, respectively. For concretes with a w/c ratio of 0.65, the carbonated and non-carbonated regions could be separated by mechanical means, allowing ρ_S and %TV to be measured in these two areas. The concrete specimens with a w/c ratio of 0.45 had very small e_{CO2} (< 5 mm) to separate both regions, so the measured value is almost that of uncarbonated concrete.

It can be seen from Figs. 9 and 10 that a layer of greater electrical resistivity and lower porosity is created in the concrete that is carbonated, so the diffusion of both CO_2 and the water necessary for the chemical reaction between CO_2 and cement hydration products is

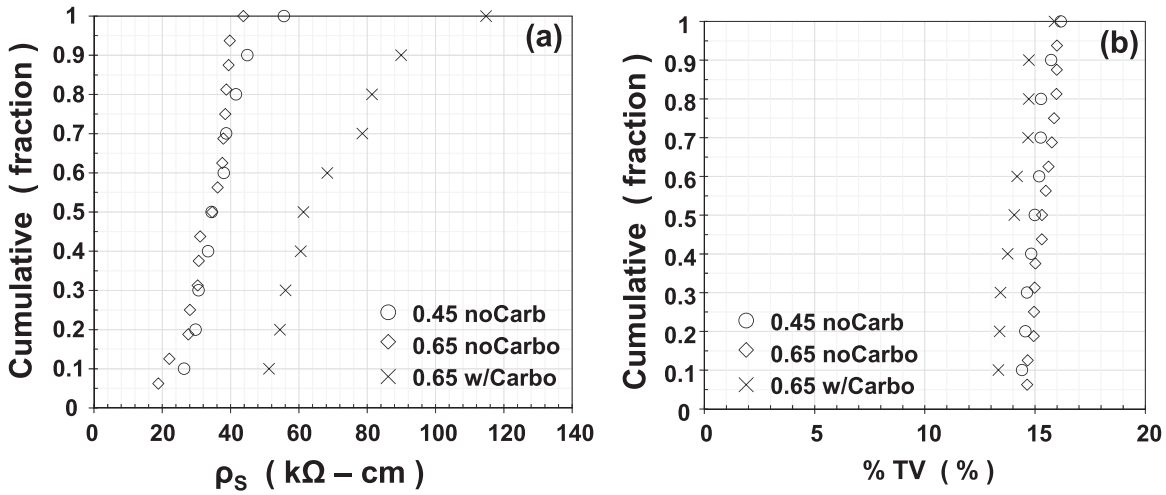

Fig. 9. Cumulative values of ρ_S and %TV for the non-carbonated concretes with w/c of 0.45 (○) and 0.65 (◊) and for the carbonated concrete with w/c of 0.65 (×) from the TOL, Mexico, test site.

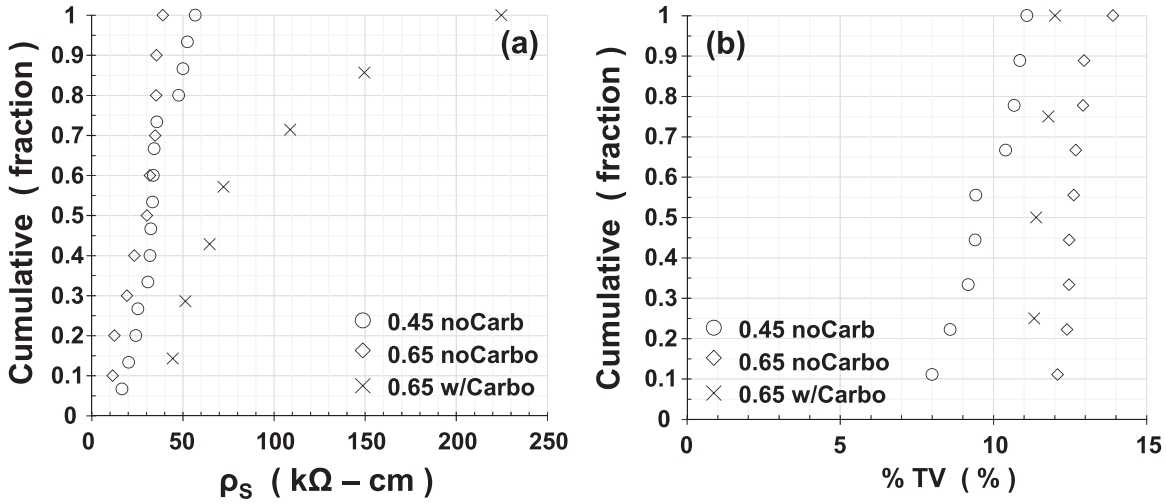

Fig. 10. Cumulative values of ρ_S and %TV for the non-carbonated concretes with w/c of 0.45 (○) and 0.65 (◊) and for the carbonated concrete with w/c of 0.65 (×) from the QRO, Mexico, test site.

slowed down. This is why the concrete with a w/c ratio of 0.65 also showed a reduction in the slope of the e_{CO2} values obtained between ~5 and ~20 years, as seen in Fig. 8.

5.3. Concrete carbonation coefficient k_{CO2} after ~20 years of natural exposure

Previous research has defined that the concrete carbonation depth e_{CO2} follows a relation similar to the square root of time (SRT) equation: $e_{CO2} = k_{CO2} \cdot t^{½}$, where k_{CO2} is known as the concrete carbonation coefficient or rate (in mm/year^{½}) and t is time (in years) [1,2,4,7,10]. Using the e_{CO2} values obtained (Figs. 7 and 8), the discretized k_{CO2} values were estimated for all monitoring sites on each date when the e_{CO2} value was measured.

Figs. 12 and 13 show how the k_{CO2} values change over time, observing an almost constant increase in the first ~2 years of continuous monitoring [27,28], a reduction in this value in the last e_{CO2} measurement at > 2 years of exposure, continuing this decrease at ~20 years. This implies that certain precautions must be taken in estimating k_{CO2} if the exposure time is < 5 years since this value could be overestimated. These results indicate that the concrete carbonation process is not constant over time and follows an equation as simple as the SRT's.

The following analysis carried out with the experimental data obtained is the estimation of k^S_{CO2}, which corresponds to the slope of e_{CO2} vs $t^{½}$ at time t (here t = 5 or 20 years), assuming that the approximation of the SRT equation is valid for all types of concrete and exposure environment. This value is known as the concrete carbonation coefficient measured with the slope of the experimental data between e_{CO2} vs $t^{½}$. Fig. 14 shows, as an example, the plots of e_{CO2} vs $t^{½}$ for the MOR (Fig. 14a), TOL (Fig. 14b), CDMX (Fig. 14c), and QRO (Fig. 14d) test sites.

The analysis was carried out using Excel, where the values of e_{CO2} vs $t^{½}$ were plotted. The software was asked to provide the trendline of the data in linear form, the equation of this trendline ($e_{CO2} = k^S_{CO2} \cdot t^{½} + b$), and the correlation coefficient R^2 of the estimate for the data presented in previous publications [27,28] and this research. Fig. 14 shows the two trendlines (at t between 1 and 5 years with continuous line; and t between 1 and ~20 years with discontinuous line) and their respective equations and R^2 for the same four test sites previously taken as examples (MOR, TOL, QRO, and CDMX). Table 5 lists the results for all 12 sites and w/c ratios wherein values after ~5 and ~20 years of exposure are tabulated separately. It is observed from this table that the k^S_{CO2} values from previously published results at the time of measurements between 2007 and 2008 [28] are greater than k^S_{CO2} estimated with the

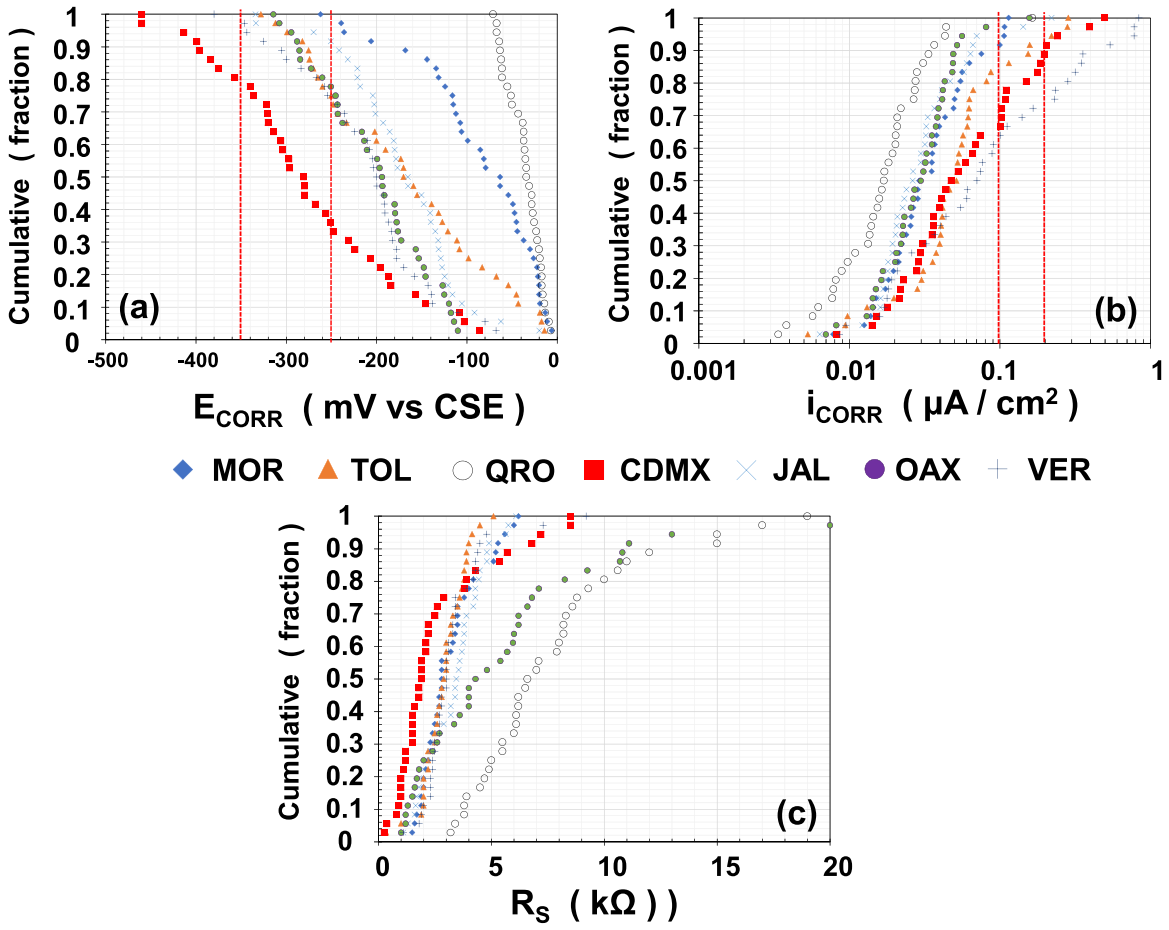

Fig. 11. Cumulative values of electrochemical parameters a) E_{corr}, b) i_{corr} of the reinforcement, and c) R_S of the concrete from seven (out of 12) natural exposure sites of the project.

Table 4
Meteorological parameters in each monitoring site from 2003 until 2017.

Urban Site	T (°C)	HR (%)	TW* (fraction)	RF (mm)	CO_2 (mg/l)
MOR	19.1	63.6	0.37	1002.6	0.76
Toluca (TOL)	8.3	69.9	0.51	1487.4	0.71
Queretaro (QRO)	16.1	60.6	0.25	621.4	0.7
Mexico City (CDMX)	17.4	44.7	0.17	1076.3	0.77
Jalapa (JAL)	20.7	70.1	0.41	1245.7	0.56
Oaxaca (OAX)	22.3	65.9	0.36	861.1	0.65
Merida (MID)	25.5	65.9	0.41	987.4	0.68
Urban/Marine Site	**T (°C)**	**HR (%)**	**TW (fraction)**	**RF (mm)**	**CO_2 (mg/l)**
Veracruz (VER)	25.4	75.2	0.5	898.4	0.76
Camp SMN	27.7	71.5	0.11	997.6	0.51
Camp ITC	27.7	71.5	0.11	997.6	0.56
Camp CRIP	27.7	71.5	0.11	997.6	0.53
Progreso (PRO)	26.9	76.0	0.46	152	0.74

* T = average annual temperature; HR = average annual relative humidity; TW = average annual wetting time (defined as the yearly time fraction during which T > 0 °C and HR > 80 %); RF = average annual cumulative rainfall; CO_2 = ambient CO_2 concentration (averages were obtained with point measurements at the time of the visit to the sites, between 3 and 20 measurements during the period between 2003 and 2017).

e_{CO2} data at ~20 years of exposure.

Fig. 15a plots the values of $k^S_{e,CO2}$ against $k^S_{t,CO2}$. As can be seen from the figure, the vast majority (22 of 24 data) of the slopes for t < 5 years ($k^S_{t,CO2}$) of reference [28] were higher than the slopes estimated with all the values obtained over the experimentation period of ~20 years. This indicates that the carbonation process shifted from the performance observed in the first ~5 years of natural exposure, which again corroborates the hypothesis that the natural exposure of the concrete specimens, without these being protected from changes in temperature and humidity over ~20 years, is affecting what the empirical SRT equation would predict in the first few years of exposure. This would produce an overestimation, which may be very high, of the e_{CO2} values if the $k^S_{t,CO2}$ value were used to predict the depth of carbonation e_{CO2} at older ages (for example, ~20 years, which is the time frame for this research).

Fig. 15b plots the values of $k^S_{e,CO2}$ (Table 5) against the values of k_{CO2} at ~20 years of exposure (Figs. 12 and 13). As can be seen from the figure, the $k^S_{e,CO2}$ values are approximately 34 % lower compared to the results obtained for k_{CO2} at ~20 years of natural exposure. However, the approximation between these two parameters, k_{CO2} at ~20 years and $k^S_{e,CO2}$, is closer than between $k^S_{t,CO2}$ and $k^S_{e,CO2}$ analyzed above. It can also be observed that the values obtained from the urban sites (○ symbols) are the furthest from the equality line shown in the figure. In contrast, the data from the urban/marine sites seem to estimate the carbonation constant indistinctly, whether it is obtained at a point in time or using the slope of the e_{CO2} vs $t^{½}$ data.

Fig. 15b also shows the abbreviated names (JAL, TOL, CDMX) of the sites that showed a performance very far from the equality line. It is observed that these sites are the highest above sea level of all the Mexican sites. This would imply that the site's altitude would generate these differences between the results of k_{CO2} and $k^S_{e,CO2}$; therefore, this must be corroborated with a larger number of data to consider this other geographical parameter.

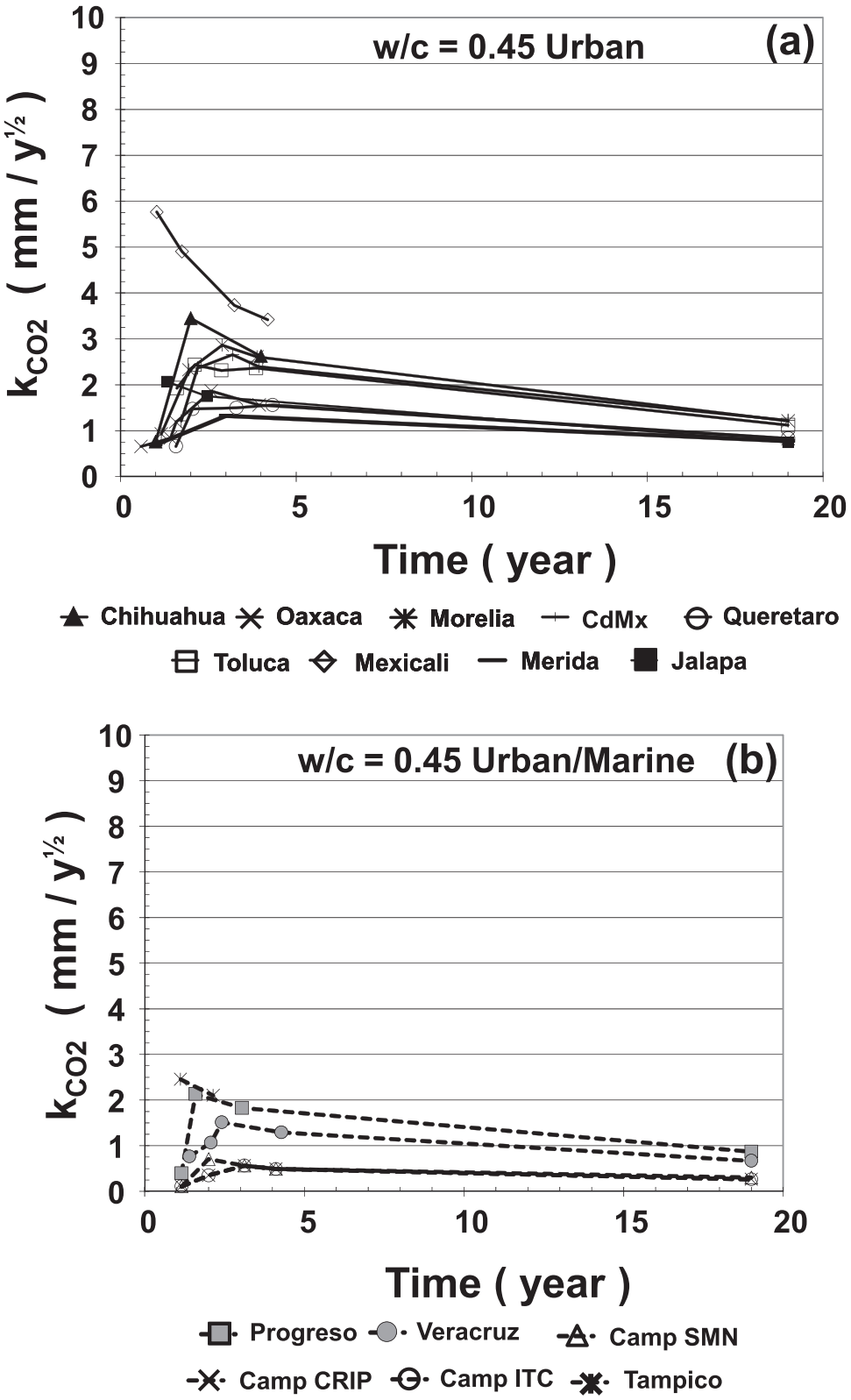

Fig. 12. Estimated values of k_{CO2} for each date that slice cutting was carried out to measure e_{CO2} for concretes with a w/c of 0.45: a) urban sites; (b) urban/marine sites.

5.4. Empirical equation to Obtain k_{CO2} as a function of environmental parameters and concrete type

Next, the k_{CO2} values at the exposure time of ~20 years are used to obtain an empirical equation that helps obtain the approximate value of k_{CO2} based on the meteorological parameters for each site evaluated in this research.

This empirical equation was obtained using the multiple linear regression tool provided by Excel. The procedure used the average meteorological data between 2003 and 2017 from each site, which are

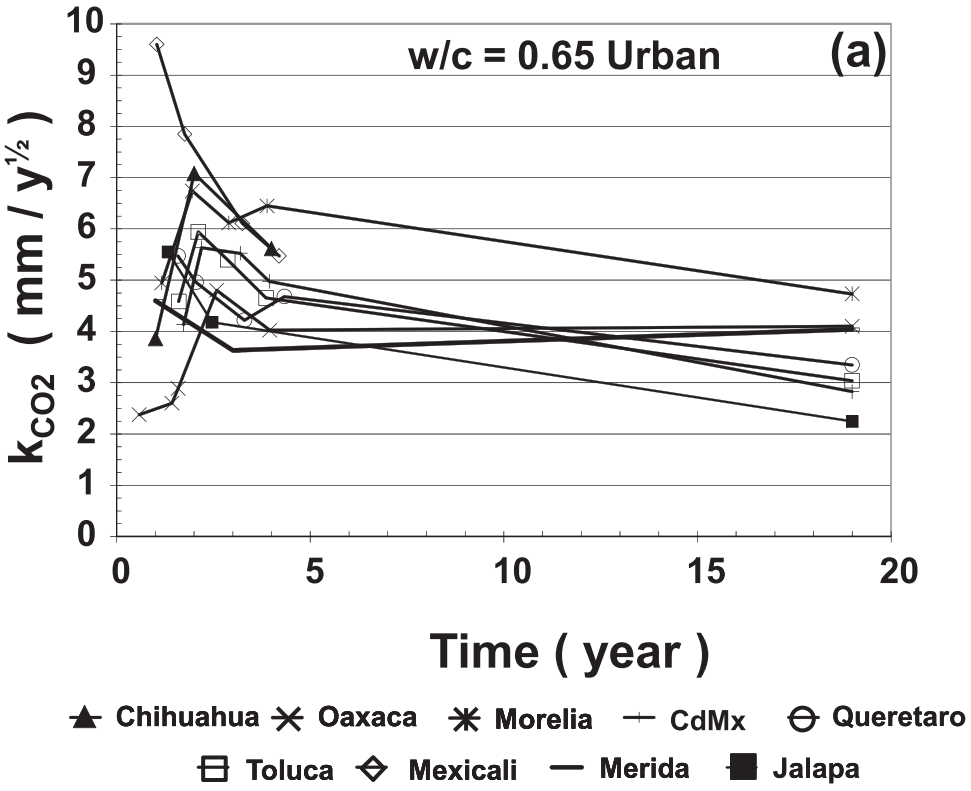

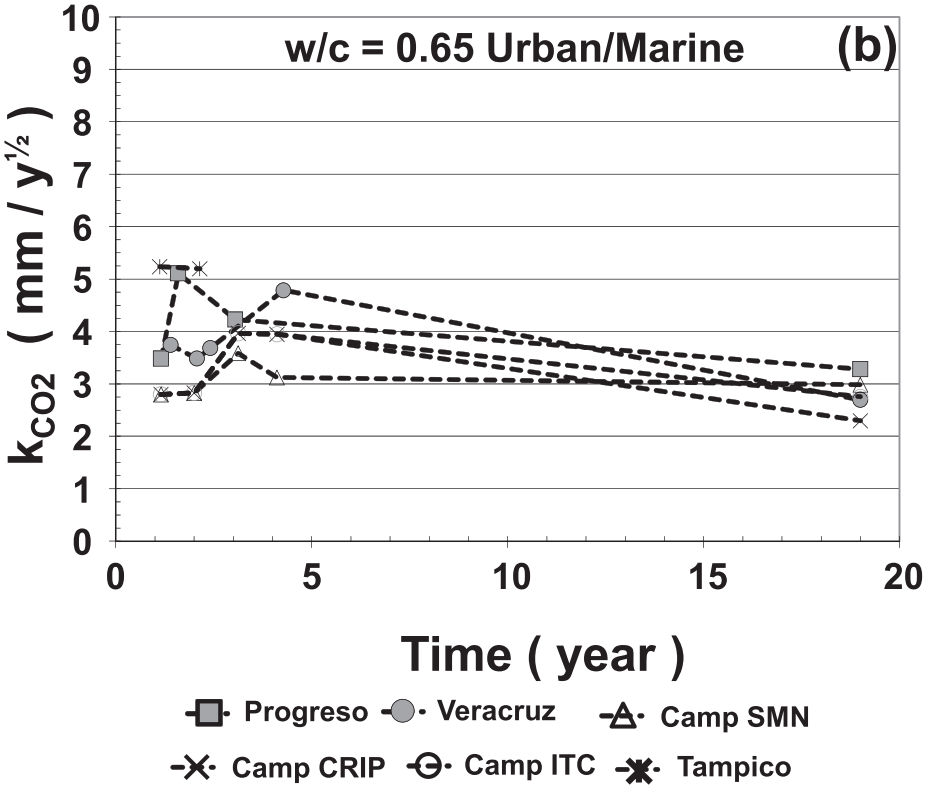

Fig. 13. Estimated values of k_{CO2} for each date that slice cutting was carried out to measure e_{CO2} for concretes with a w/c of 0.65: a) urban sites; (b) urban/marine sites.

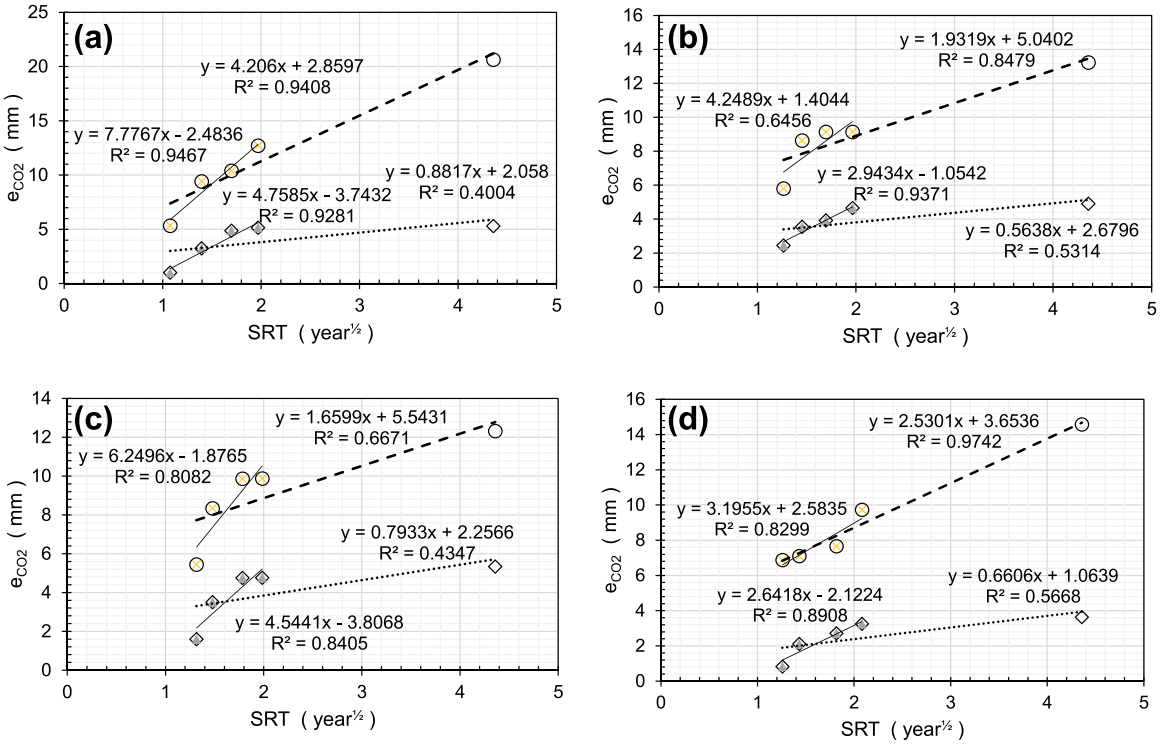

Fig. 14. Correlations obtained between e_{CO2} and $t^{1/2}$ for each natural exposure site and type of concrete (w/c of 0.45 and 0.65): a) MOR; (b) TOL; (c) CDMX; and (d) QRO.

Table 5
Values of k^S_{CO2}, constant b, and regression coefficient R^2 of the empirical equations obtained from the slopes of e_{CO2} against time at 5 [21] and ~20 years for each evaluated site and concrete type.

Urban Site	0.45			0.65		0.45				0.65		
	k^S_{CO2} (mm/year½)	b_5 *	R^2_5	k^S_{CO2} (mm/year½)	b_5	R^2_5	k^S_{20CO2} (mm/year½)	b_{20}	R^2_{20}	k^S_{20CO2} (mm/year½)	b_{20}	R^2_{20}
MOR	4.759	3.74	0.928	7.777	2.48	0.947	0.882	2.06	0.4	4.206	2.86	0.400
TOL	2.943	1.05	0.937	4.249	1.40	0.646	0.564	2.68	0.531	1.932	5.04	0.848
QRO	2.642	2.12	0.891	3.196	2.58	0.83	0.661	1.06	0.567	2.53	3.65	0.974
CDMX	4.544	3.81	0.841	6.25	1.88	0.808	0.793	2.26	0.435	1.66	5.54	0.667
JAL	0.882	1.37	1.000	0.405	5.91	1.000	0.244	2.22	0.909	1.095	4.99	0.994
OAX	2.413	1.46	0.894	5.491	2.82	0.952	0.779	0.67	0.619	4.523	1.56	0.987
MID	2.172	1.47	1.000	2.295	2.31	1.000	0.703	0.47	0.836	3.987	0.07	0.992
Urban/Marine Site	**0.45**			**0.65**		**0.45**				**0.65**		
	k^S_{CO2} (mm/year½)	b_5	R^2_5	k^S_{CO2} (mm/year½)	b_5	R^2_5	k^S_{20CO2} (mm/year½)	b_{20}	R^2_{20}	k^S_{20CO2} (mm/year½)	b_{20}	R^2_{20}
VER	1.95	1.17	0.824	6.49	3.86	0.949	0.477	1.07	0.539	2.246	2.60	0.79
Camp SMN	0.826	0.58	0.636	3.889	1.19	0.923	0.25	0.35	0.494	2.975	0.20	0.982
Camp ITC	1.012	0.94	0.934	5.611	3.31	0.962	0.247	0.23	0.528	2.584	1.30	0.886
Camp CRIP	1.012	0.94	0.934	5.611	3.31	0.962	0.247	0.23	0.528	1.922	2.31	0.75
PRO	3.502	2.66	0.682	4.724	0.57	0.751	0.666	1.12	0.477	2.884	1.88	0.957

* Dimensionless values.

listed in Table 4, along with the k_{CO2} values for each type of concrete and each exposure site found in Figs. 12 and 13. Being a linear regression tool, the base-ten logarithms of the experimental values were estimated to perform this regression using this equation:

$$\text{Log } k_{CO2} = A \text{ Log (T)} + B \text{ Log (HR)} + C \text{ Log (TW)} + D \text{ Log } (CO_2) + E \text{ Log } (\rho_S) + \text{const} \quad (2)$$

Once the values of constants A-E of each parameter used as a variable were obtained, the empirical equation was obtained by transforming it into a series of multipliers whose sign would define whether they were placed in the numerator or denominator of the equation.

The regression generated the following linear equation (rounded to three decimal places):

$$\text{Log } k_{CO2} = -0.067 \text{ Log (T)} - 0.981 \text{ Log (HR)} + 0.324 \text{ Log (TW)} + 0.660 \text{ Log } (CO_2) - 2.930 \text{ Log } (\rho_S) + 6.668 \quad (3)$$

The factors of this empirical equation are ordered using the rule of logarithms, giving the following equation:

$$k_{CO2} = \frac{4.7 \bullet 10^6 \bullet TW^{0.32} \bullet CO_2{}^{0.66}}{\rho_S{}^{2.93} \bullet T^{0.07} \bullet HR} \quad (4)$$

Fig. 16 compares the experimental value of k_{CO2} at ~20 years with the one estimated using Eq. (1). The same figure shows the correlation equation between both values and the corresponding correlation coefficient R^2. As can be seen, the R^2 coefficient was relatively high (0.8136).

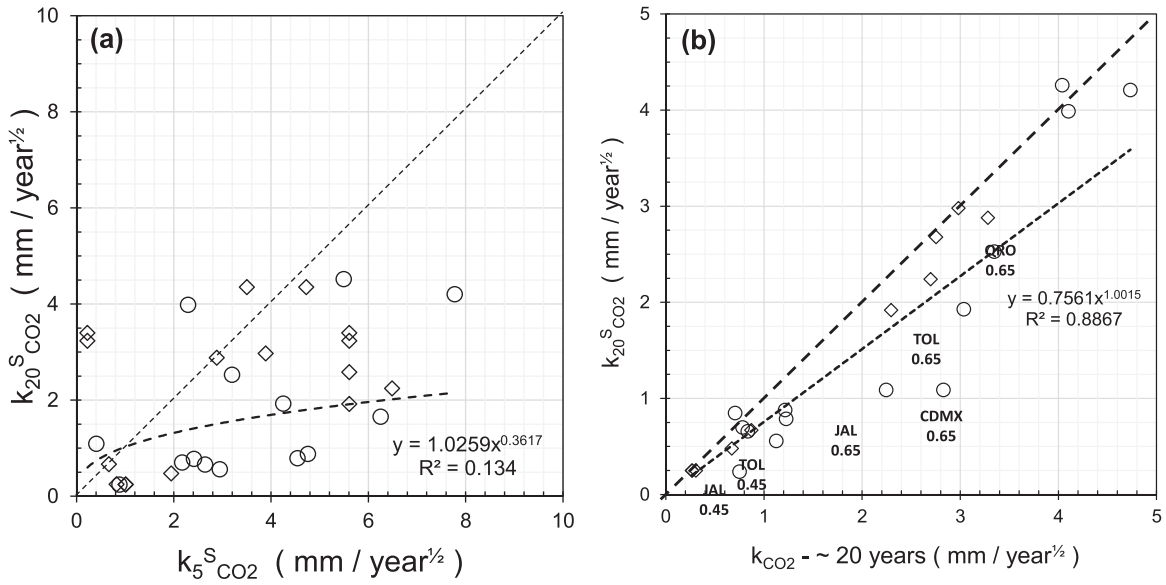

Fig. 15. Correlations between a) the values of k^{S}_{5CO2} and k^{S}_{20CO2} corresponding to the ~5-year and ~20-year slopes, respectively, of the e_{CO2} versus $t^{1/2}$; b) the estimated values of ~20-year k_{CO2} and k^{S}_{20CO2} for each urban (○) and urban/marine (◇) site.

The values that deviated from the equality line (indicated in Fig. 16 with the abbreviations of the sites' names) were those corresponding to the concrete with a w/c ratio of 0.65, observing an overestimation of the k_{CO2} carbonation coefficient for the urban sites and an underestimation for two of the urban/marine test sites located in Campeche.

5.5. *Carbonation coefficient based on the empirical equation of the form* $e_{CO2} = k'_{CO2}\cdot t^{n}$

The carbonation coefficient k_{CO2} was estimated previously using the empirical equation of the SRT. In this section, an empirical equation is obtained to approximate better the values of e_{CO2} and t^{n}, where n is not a fixed exponent equal to ½, but a parameter determined by multiple regression analysis. The proposed empirical equation has an exponential form as follows: $e_{CO2} = k'_{CO2}\cdot t^{n}$, where n is the time power that is estimated from multiple regression analysis of the data obtained experimentally at each site. The e_{CO2} and t values obtained at each site, for both concretes with w/c ratios of 0.45 and 0.65, were entered into an Excel spreadsheet to estimate the k'_{CO2} and n values by multiple regression for each site and type of concrete, as well as their corresponding correlation coefficients.

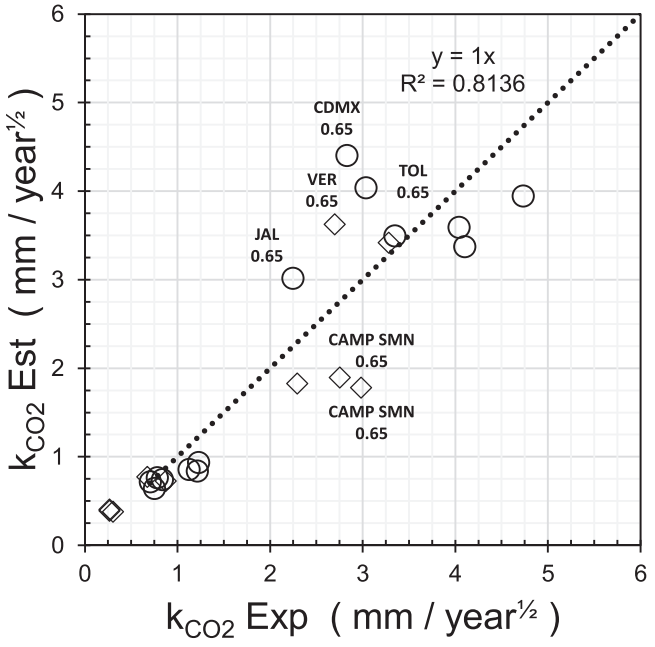

Fig. 16. Experimental values of k_{CO2} against those estimated with Eq. (1).

As an example, Fig. 17 shows the graphs of the results of the four test sites that have been included in this research: MOR (Fig. 17a), TOL (Fig. 17b), CDMX (Fig. 17c), and QRO (Fig. 17d). This figure shows the experimental e_{CO2} data obtained as points on the graph at the different slice-cutting times at the four mentioned sites. In addition, the correlation exponential trendlines can also be seen in the figures, along with the trend equations $e_{CO2} = k'_{CO2}\cdot t^{n}$ and the correlation coefficients R^2. These lines and correlation equations were obtained using the spreadsheet for each site (the three sites that stopped operating after ~5 years of this investigation are not included in the analysis).

The results of these correlation analyses are shown in Table 6 for each site and concrete type. Noting that the correlation equation obtained is of the form $e_{CO2} = k'_{CO2}\cdot t^{n}$, Table 6 shows the values of k'_{CO2} and n for each site and concrete type, separating these results by type of site: urban or urban/marine. The field sites used to obtain the values in Table 6 include all the sites except those three that stopped operating ~5 years after starting the project (MEX, CHI, and TAM).

From the values of the exponential equation used as an approximation for the data obtained from e_{CO2} vs t for each site and type of concrete (listed in Table 6), better correlation coefficients R^2 are observed for the concrete data with a w/c of 0.65 (between 0.806 and 0.969) compared to the concrete with a w/c ratio of 0.45 (between 0.426 and 0.829). This may be due to this re-alkalization effect that drastically reduces the final carbonation front depth of the concrete element after ~20 years.

It is worth mentioning that the values of the exponent n vary between 0.11 and 0.73 for the concrete with a w/c ratio of 0.45 and between 0.17 and 0.67 for the concrete with a w/c ratio of 0.65. Only three out of 24 possible values of n are in the range n=0.5±0.05, which would correspond to the exponent of the SRT ($t^{½}$) for both concretes, i.e., only 12.5 % of the total sites evaluated are within a range close to the n value of ½ corresponding to the empirical SRT equation that has been used for many years to simulate concrete carbonation.

Fig. 18 compares the values of k_{CO2} and k'_{CO2} for each site and type of concrete, showing there is an important difference between the

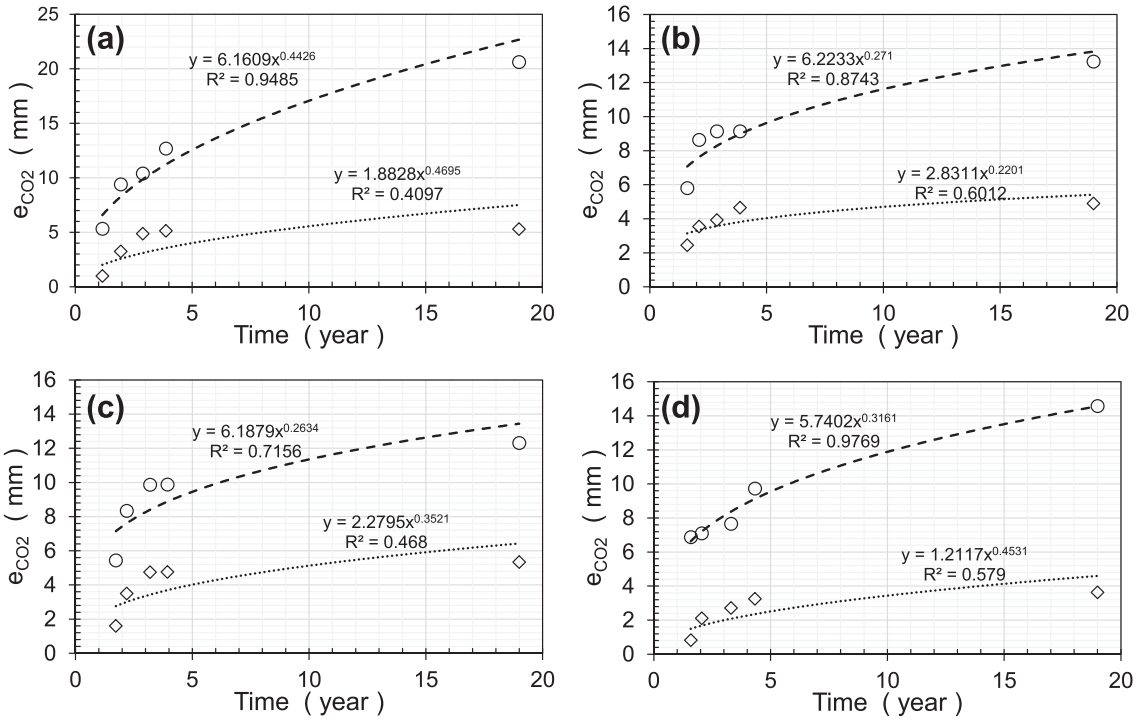

Fig. 17. Correlations obtained between e_{CO2} and t for each natural exposure site and type of concrete with w/c of 0.45 (◊) and 0.65 (○): a) MOR; (b) TOL; (c) CDMX; and (d) QRO.

Table 6
Values of k'_{CO2}, exponent n, and regression coefficient R^2 of the empirical equations (exponential type) of e_{CO2} against time for each evaluated site and concrete type.

Urban Site	0.45			0.65		
	k'_{CO2} (mm/year^n)	n_{CO2} (*)	R^2	k'_{CO2} (mm/year^n)	n_{CO2}	R^2
MOR	1.883	0.49	0.494	6.161	0.44	0.909
TOL	2.831	0.22	0.593	6.223	0.27	0.806
QRO	1.2112	0.45	0.553	5.740	0.32	0.965
CDMX	2.280	0.35	0.454	6.188	0.26	0.657
JAL	2.385	0.11	0.941	5.882	0.17	0.971
OAX	1.015	0.57	0.738	2.853	0.67	0.942
MID	0.893	0.50	0.829	4.257	0.47	0.976
Urban/ Marine Site	**0.45**			**0.65**		
	k'_{CO2} (mm/year^n)	n_{CO2}	R^2	k'_{CO2} (mm/year^n)	n_{CO2}	R^2
VER	1.210	0.36	0.583	4.162	0.39	0.844
Camp SMN	0.279	0.69	0.464	2.977	0.51	0.969
Camp ITC	0.225	0.73	0.563	3.234	0.49	0.882
Camp CRIP	0.225	0.73	0.563	3.402	0.43	0.798
PRO	1.047	0.53	0.426	4.356	0.42	0.901

* Dimensionless value.

carbonation coefficients obtained based on the empirical equation $e_{CO2} = k_{CO2} \cdot t^{1/2}$ (SRT) and the empirical equation $e_{CO2} = k'_{CO2} \cdot t^n$. The values of k_{CO2} are lower than those of k'_{CO2} by approximately 37 %. However, the carbonation front e_{CO2} no longer depends on the value of k'_{CO2} alone but also on the exponent n of the empirical equation. This is the reason to continue estimating the empirical equation to obtain k'_{CO2} and n based on the environmental parameters and type of concrete.

5.6. Empirical equation of k'_{CO2} as a function of environmental parameters and concrete type

As previously explained, this new empirical equation was obtained following the same procedure to obtain k_{CO2} using Excel's multiple linear regression tool. The regression generated the following linear equation for k'_{CO2} (rounding to three decimal places):

$$\text{Log } k'_{CO2} = -0.514 \text{ Log}(T) - 2.063 \text{ Log}(HR) + 0.713 \text{ Log}(TW) - 0.410 \text{ Log}(CO_2) - 2.909 \text{ Log}(\rho_S) + 9.380 \quad (5)$$

The factors of this empirical equation are ordered using the rule of logarithms, giving the following equation:

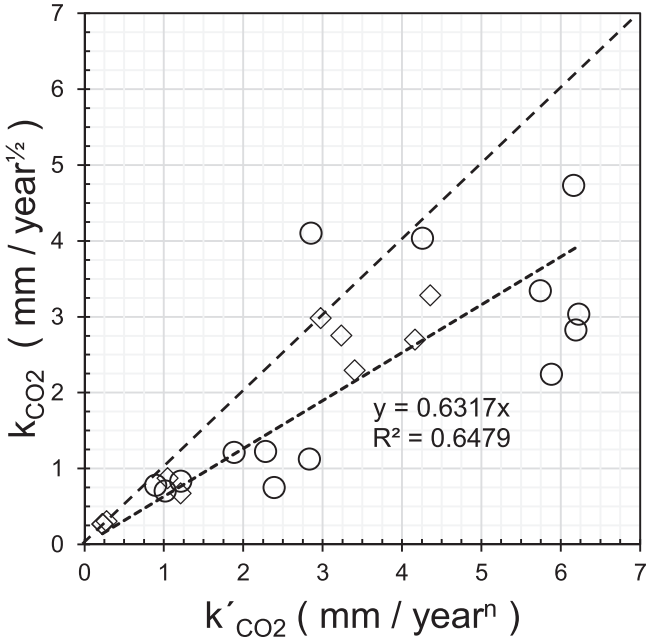

Fig. 18. Correlation between the estimated values of k_{CO2} at ~20 years and k'_{CO2} for each urban (○) and urban/marine (◊) site.

$$k_{CO2}^{'} = \frac{2.24 \bullet 10^{9} \bullet TW^{0.713}}{\rho_S^{2.93} \bullet T^{0.514} \bullet CO_2^{0.41} \bullet HR^{2.063}} \quad (6)$$

The linear equation obtained for n is given by:

$$\text{Log n} = 0.446\ \text{Log(T)} + 1.692\ \text{Log(HR)} - 0.668\ \text{Log(TW)} + 2.354\ \text{Log}(CO_2) + 0.219\ \text{Log}(\rho_S) - 4.338 \quad (7)$$

The factors of this empirical equation are ordered using the rule of logarithms, giving the following equation:

$$n = \frac{5.102 \bullet 10^{-5} \bullet T^{0.446} \bullet HR^{1.692} \bullet CO_2^{2.354} \bullet \rho_S^{0.219}}{TW^{0.668}} \quad (8)$$

Fig. 19 compares the experimental values of k'_{CO2} and n with those estimated using Eqs. (6) and (8), as well as the correlation equations and the corresponding correlation coefficients R^2 of experimental and estimated values. As seen in this figure, the correlation coefficient between the experimental and estimated values for the variable k'_{CO2} is quite good (0.8127); however, the R^2 coefficient is 0.2018 for the variable n, which suggests that Eq. (8) does sufficiently approximate n to be applied at this time. The exponent n must be evaluated with more experimental data obtained in the same way with concrete specimens exposed to a natural environment and without being sheltered from inclement weather.

Fig. 20 presents the empirical correlations between k'_{CO2} and n for w/c=0.45 (◊: dark symbol for urban and white symbol for urban/marine) and w/c= 0.65 (○: dark symbol for urban and white symbol for urban/marine) concretes. As observed in this figure, both data groups and their correlation coefficients were quite different, showing an almost linear relationship between k'_{CO2} and n for 0.65 w/c ratio concrete data, and SRT relation for 0.45 w/c ratio concrete data. This must be corroborated with a larger number of data to consider a possible trend with these two empirical parameters, k'_{CO2} and n.

5.7. Electrochemical behavior of reinforcing steel after ~20 years of exposure

The results of the electrochemical monitoring after ~20 years of exposure are shown in Fig. 11 (for monitoring results from previous years, see reference [27]). This figure includes the cumulative values of the three parameters that the measuring equipment collects in each test: E_{corr}, i_{corr}, and R_S. Fig. 11a shows that the measured values of E_{corr} in specimens from the CDMX site were the most active, with the most negative half-cell potential recorded from all the field sites. Of these measurements, 20 % of the values corresponded to a 95 % probability of corrosion activation (< −350 mV vs CSC) according to ASTM C-876 [20]; 50 % in the range of 50 % probability of corrosion (between −250 and −350 mV vs CSC) [20]; and only 30 % in the range of values of 20 % probability of corrosion [20]. The values obtained at the VER and OAX sites follow these half-cell potential measurements. The field sites that showed the most passive values of E_{corr} were those of QRO and MOR.

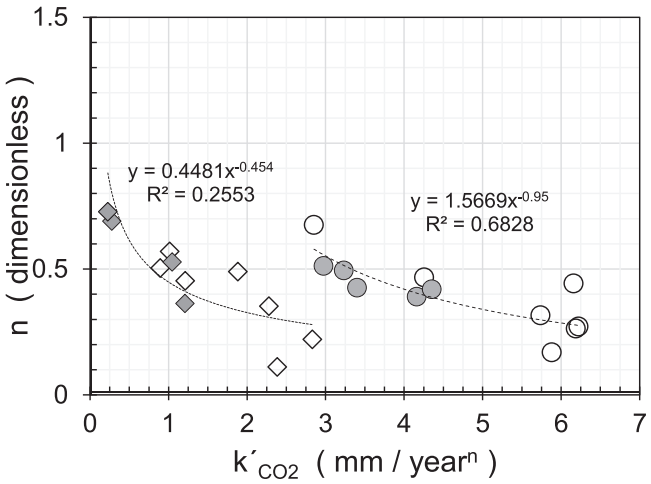

Fig. 20. Correlation between k'_{CO2} and n for each urban (○) and urban/marine (◊) test sites. Filled symbols correspond to urban test sites, and unfilled symbols for urban/marine test sites.

By reviewing the values of i_{corr} in Fig. 11b, it is noted that the most active values were measured at the VER, CDMX, and TOL sites in that order. The results indicate that the reinforcing steels in the specimens at the VER site were more active than those at CDMX, even though more negative values of E_{corr} were measured at CDMX compared to VER. This is possibly because the concretes in VER are more contaminated by chloride ions than those in CDMX, generating greater corrosion activation in the VER site. The lowest i_{corr} values (more passive) were those obtained at the QRO site, corroborating what was seen with the results obtained from E_{corr}.

Finally, the R_S values measured at the seven sites and shown in Fig. 11c follow an inverse pattern to that found with the i_{corr} values: the concretes with the highest electrical resistance were those of the QRO site, followed by OAX, VER, and lastly CDMX. This agrees with previous observations, wherein i_{corr} is inversely proportional to concrete's R_S.

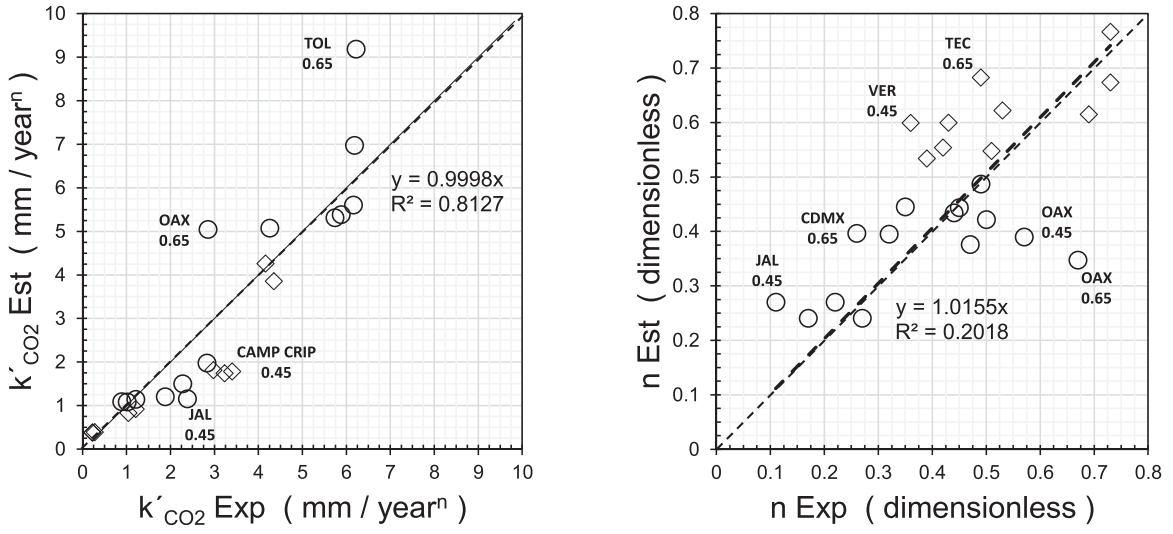

Fig. 19. Correlation between experimental values of k'_{CO2} and n against those calculated using Eqs. (2) and (3) for each urban (○) and urban/marine (◊) site.

Fig. 21 plots all the electrochemical data to determine possible correlations between these values: E_{corr} vs i_{corr} and R_S vs i_{corr}. Also shown in Fig. 21a are red dotted lines that delimit the evaluation criteria defined in reference [20] Standard for half-cell potential E_{corr} and current intensity i_{corr} evaluation criteria defined in references [1] and [7], to determine whether the reinforcing steel is active or passive due to corrosion.

From Fig. 21a, the following is observed:

1. Only 0.7 % of the measurements fall in the range of $E_{corr} < -350$ mV vs CSC [20], and $i_{corr} > 0.2$ μA/cm^2 [1,7]: 95 % probability due to active corrosion.
2. 3.7 % of the measurements fall in the range of $E_{corr} > -350$ mV vs CSC [20], and $i_{corr} > 0.2$ μA/cm^2 [1,7]: 50 % probability due to active corrosion.
3. 3.2 % of the measurements fall in the range of $E_{corr} < -350$ mV vs CSC [20], and $i_{corr} < 0.2$ μA/cm^2 [1,7]: 50 % probability due to active corrosion.
4. 7.4 % of the measurements fall in the range of $-250 < E_{corr} < -350$ mV vs CSC [20], and $i_{corr} < 0.2$ μA/cm^2 [1,7]: 50 % probability due to active corrosion.
5. 85 % of the measurements fall in the range of $E_{corr} < -250$ mV vs CSC [20], and $i_{corr} < 0.2$ μA/cm^2 [1,7]: the reinforcing steel is passive.

This corroborates what was obtained with the e_{CO2} measurements; three of the 12 sites presented carbonation fronts deeper than 15 mm for the concretes with a w/c ratio of 0.65. This implies that 12.5 % of the concrete specimens should present activation by corrosion in the reinforcing steel, which agrees with the 15 % activated obtained from direct

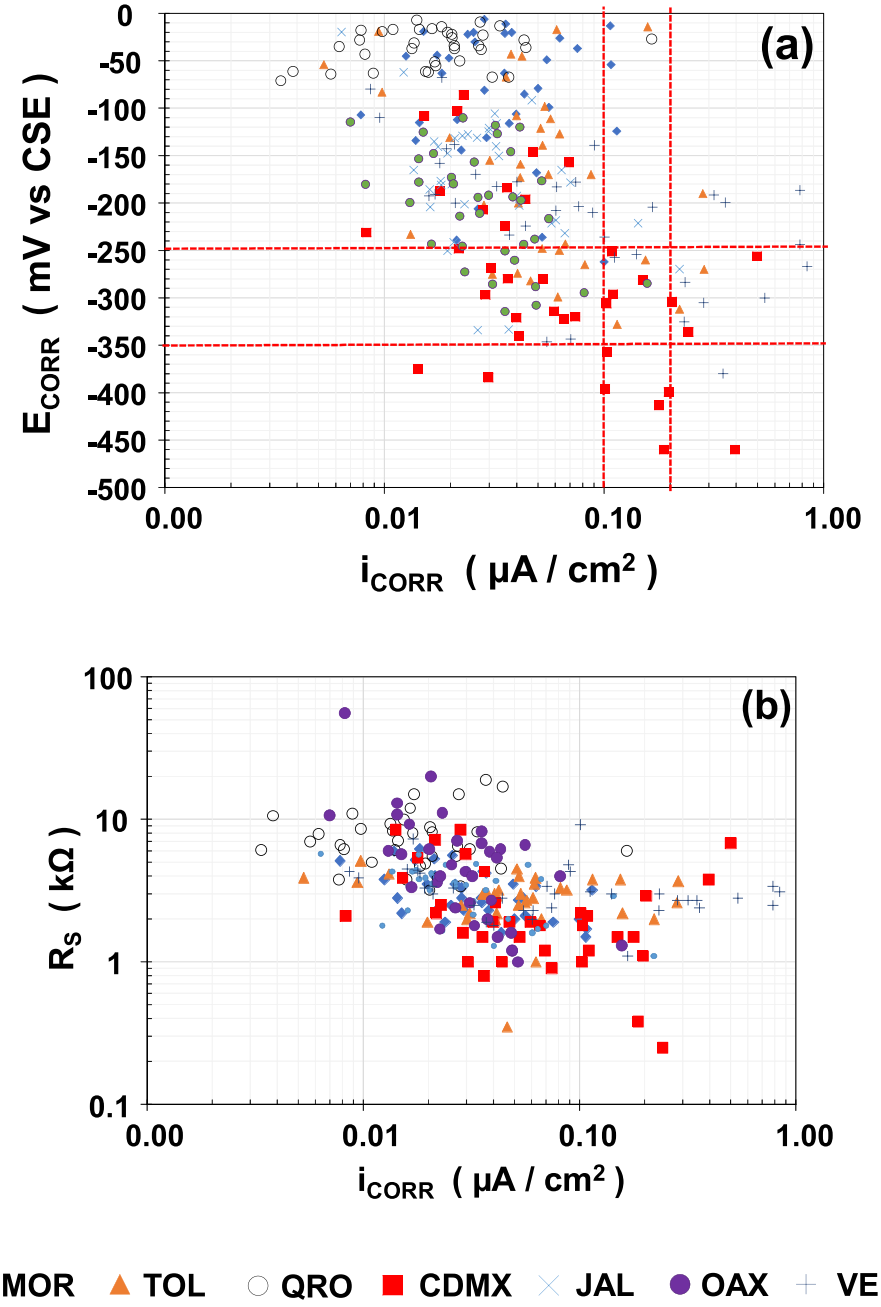

Fig. 21. Electrochemical parameters in seven of the exposure sites of the project: (a) E_{corr} vs i_{corr} and (b) R_S vs i_{corr}.

electrochemical measurements.

Fig. 21b shows the correlation between the values of i_{corr} and R_S. A distinct trend is observed in which R_S is inversely proportional to i_{corr}, a relation previously observed between the values of electrical resistivity of concrete (ρ) and i_{corr} [29,30]. It is worth mentioning that the measuring equipment gave the obtained R_S values that correspond to the electrical resistance of the concrete cover to the passage of the polarization current at the time of performing the electrochemical measurement. This electrical resistance depends not only on the thickness of the cover (the same for all the specimens evaluated) but also on the internal humidity of the pores of the concrete itself. The variation between the values may be because the measurements were carried out at different times of the year, at which the R_S values of the concrete specimens could have been influenced by the degree of ambient humidity that prevailed at the time of measurement.

The electrochemical values (E_{corr} and i_{corr}) measured at the QRO site are the least active due to corrosion. Also, the measurements of R_S are the highest of all the field sites, being congruent with the meteorological parameters at the site, as the city of QRO was the one that showed the lowest RH and RF of all the Mexican test sites, and it had an atmospheric CO_2 concentration between intermediate and high. This would imply that this city is the least aggressive due to carbonation compared to the rest.

On the other hand, the cities that showed the most significant activity due to reinforcement corrosion were CDMX and VER, with the highest i_{corr} values, the most negative values of E_{corr}, and the lowest values of R_S. The case of CDMX is not surprising, as it is one of the cities with the highest population density in the world and a large number of industrial areas in the country, making it an environment with a high concentration of aggressive agents such as CO_2 that can react with the concrete by carbonating it and with enough ambient humidity to activate the reinforcing steel, as observed from the low R_S values of the concrete.

Active values of E_{corr} and i_{corr} were also observed in the city of VER; however, the measured values of the concrete R_S lie in an intermediate zone in Fig. 21b compared to those measured at the CDMX site, which lie on the bottom region of Fig. 21b. This implies that chloride contamination in the VER site's concrete specimens was insufficient to reduce the concrete R_S as occurred at the CDMX site. Although the i_{corr} values measured at the VER site were among the highest, chloride ions had not yet managed to completely activate the reinforcing steel of these specimens due to the electrical resistivity of the concrete, which was still in an intermediate range. Longer exposure time would be necessary for concrete specimens at the VER site to become more contaminated by environmental chloride ions, decreasing the concrete R_S and leading to more negative values of E_{corr}, thus allowing a higher degree of corrosion.

It is important to note that of all the specimens placed in all the field test sites in Mexico, only those located at the VER site, which was an urban/marine site, showed concrete cracking due to corrosion of the reinforcing steel. Concrete specimens located in the other urban/marine sites (SMN, TEC, CRIP, and PRO) showed no signs of corrosion-induced cracking on their surface. Fig. 22 shows the pictures taken of the three concrete specimens with a w/c ratio of 0.65 that showed reinforcement corrosion-induced cracks along three of their six reinforcing bars with a cover of 15 mm. The reinforcing bars with 20- and 30-mm covers did not show corrosion-induced cracks at the time of the evaluation (~20 years). It is worth mentioning that several marine sites of the Ibero-American DURACON Project are already active due to corrosion [3], and the case of the urban/marine sites in Mexico is particular as they are located far from the coast, and there are possible barrier effects that prevented a high-chloride airborne concentration, so the fact that these Mexican test sites have specimens that are still passive must be taken

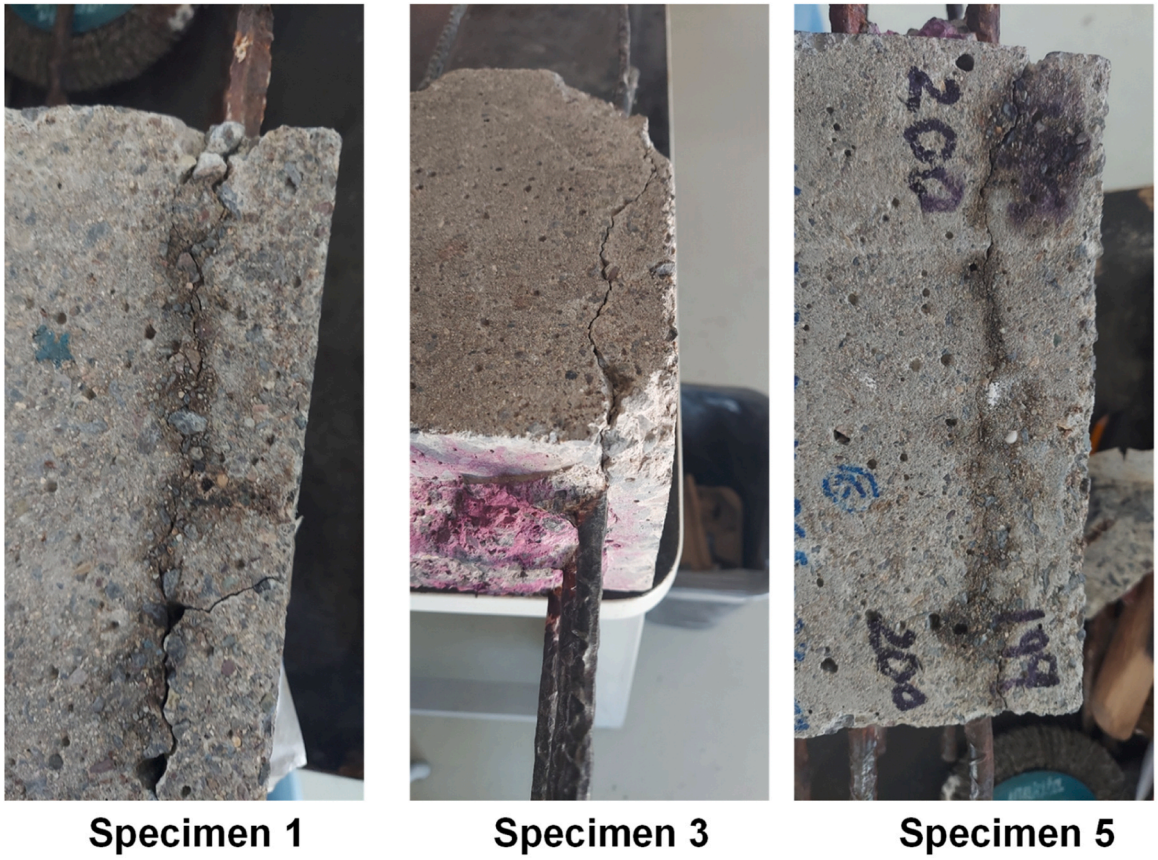

Fig. 22. Reinforcement corrosion-induced cracking in specimens at the VER exposure site. Cracks appeared only in concrete specimens with a w/c of 0.65 and the lowest concrete cover of 15 mm.

with great care.

It was expected that marine sites would display signs of deterioration due to corrosion earlier since these specimens were exposed not only to the ambient CO_2 of the place but also to chloride ions, making the environments of these sites more aggressive. However, in the case of the Campeches marine sites (SMN, TEC, and CRIP), it was observed that the wind direction was from land to sea, opposite to what it was believed the specimens would be exposed to. This reduced possible chloride contamination in the concrete as the main winds were in the opposite direction to what was supposed: from sea to land.

In the case of the PRO urban/marine site, similarly, its location did not help the exposure environment to be as aggressive as that of the VER site; since it is located 1.5 km from the coast, the exposure to chloride ions was not so aggressive. Likewise, the site is in a mangrove forest, protecting the specimens from the winds that could carry airborne chlorides. This means only the VER site showed signs of deterioration due to reinforcement corrosion in the concrete with a high w/c ratio (0.65) after an exposure period of ~20 year.

6. Conclusions

1. It was observed that, after ~20 years of exposure, the concretes presented a significant carbonation state, mainly those with a w/c ratio of 0.65 corresponding to the concrete with the highest porosity. The carbonation of the concretes with a w/c ratio of 0.45 was much lower, and this could have been due to exposure to wetting and drying cycles since the specimens were not protected from the rain and cyclical changes in humidity between day and night, which might have prevented CO_2 from diffusing inside this concrete type. The hypothesis of self-re-alkalinization could be also involved in the carbonation process in 0.45 w/c ratio concrete but was not fully demonstrated with the experimental program used in this investigation.
2. The depths of the carbonation front in specimens at the urban sites were higher than the values measured in the urban/marine sites. This could be due to the hygroscopic nature of the chloride ions present in the latter, increasing the internal humidity of the concrete, thus reducing the transport of CO_2 in its pores. However, this hypothesis needs to be demonstrated in the near future with additional experimentation.
3. In this study, it was observed that the climatological parameters that most affected concrete carbonation were the relative humidity of the environment and the direct exposure to wetting and drying cycles due to the humidity itself and/or rainfall. This reduced the carbonation rates in the concretes to such a degree in those with a low w/c ratio (0.45) that the carbonation process apparently halted and did not follow the typical empirical relationship of the square root of time (SRT) that is regularly used to estimate the depth of carbonation (e_{CO2}).
4. It was determined that if the approximation of the slope of the carbonation depth (e_{CO2}) versus $t^{½}$ is used according to the empirical SRT equation for an exposure < 5 years, the e_{CO2} values at older ages would be overestimated by almost double the actual value. This would happen if the concrete specimen were exposed to an environment that presents variations in temperature and humidity and is directly exposed to rain throughout the exposure time.
5. This condition of natural exposure without protection from changes in temperature, humidity, and rain produced a significant reduction in the carbonation of the concretes with a w/c ratio of 0.45 and a minor reduction in the concretes with a w/c ratio of 0.65. It is hypothesized that this reduction was due to a re-alkalinization process of the concrete when it is subjected to absorption/desorption of water because of rain or humidity cycles between day and night. Alkaline products at a greater depth than the carbonation front of the concrete itself could be transported out of the concrete specimen when it dries due to solar radiation or dry seasons.
6. Since the results obtained did not follow the carbonation process proposed by the empirical equation of the SRT, a new empirical equation of the form $e_{CO2} = k'_{CO2} \cdot t^n$ was proposed, and the parameters k'_{CO2} and n were estimated through multiple regression for each site of the project. The results showed that only 3 values of n of 24 (12.5 %) were close to ½, corresponding to the empirical SRT equation. This suggests that using the SRT equation should be questioned when the concrete is exposed to natural environments with wetting and drying cycles and variable temperatures.
7. This research has proposed two empirical equations to respectively obtain the parameters k'_{CO2} and n as a function of the environmental temperature (T), relative humidity (RH), time of wetness (TW), and CO_2 concentration, as well as the saturated electrical resistivity (ρ_S) of the concrete. Using the logarithms of these environmental variables, the equation obtained from multiple linear regression generated approximations of k'_{CO2} very close to those obtained from the experimental values with a correlation coefficient R^2 of 0.8127, making it an approximation that could be applied to multiple natural environments.

CRediT authorship contribution statement

Andres Antonio Torres-Acosta: Writing – review & editing, Writing – original draft, Visualization, Validation, Supervision, Resources, Project administration, Methodology, Investigation, Formal analysis, Data curation, Conceptualization. **José Pérez-Quiroz**: Methodology, Investigation, Data curation. **Saúl Crespo-Sánchez**: Methodology, Data curation. **Joel Moreno-Herrera**: Data curation. **Celene Arista-Perrusquía**: Data curation. **Demetrio Nieves-Mendoza**: Data curation. **Tezozomoc Pérez-López**: Methodology, Investigation, Data curation. **Erick Maldonado-Bandala**: Data curation. **Cipriano Bernabé**: Methodology, Data curation. **Laura Landa-Ruiz**: Conceptualization. **Elia Alonso-Guzmán**: Methodology, Investigation, Data curation. **Miguel Ángel Baltazar-Zamora**: Data curation. **Wilfrido Martínez-Molina**: Methodology, Investigation, Data curation. **Francisco Rodríguez-Gómez**: Conceptualization. **Beatriz Martín-Pérez**: Writing – review & editing, Validation, Investigation, Formal analysis, Data curation. **José Rodríguez-Campos**: Data curation. **Pedro Castro-Borges**: Writing – review & editing, Validation, Methodology, Investigation, Conceptualization. **Carlos Juárez-Cruz**: Data curation. **Oladis Troconis**: Writing – review & editing, Validation, Supervision, Project administration, Methodology, Investigation, Funding acquisition, Formal analysis, Data curation, Conceptualization. **Esteban López-Vázquez**: Conceptualization. **Abraham López-Miguel**: Data curation.

Compliance with ethical standards

None.

Funding

This study was funded by CYTED (Ciencia y Tecnología para el Desarrollo), Spain, in year 2000. Funding was provided to the International Coordinator, Dr. Oladis Troconis de Rincón and was used for mobility of the members of this DURACON Ibero American Project from 2000 to 2005. During the years 2022-2024 the project was funded by Tecnologico de Monterrey from Project Seed named "Impact of Climate Change on Carbonation Resistance of Eco-Friendly Concretes," Pep: IJST070-21OT10001-004-01, CECO: Ceco: 0700201B03.

Declaration of Competing Interest

The authors declare that they have no known competing financial interests or personal relationships that could have appeared to influence the work reported in this paper.

Data availability

Data will be made available on request.

References

[1] Manual of Inspecting, in: O. Troconis de Rincón (Ed.), Evaluating, and Diagnosing Corrosion of Reinforced Concrete Structures, second ed., CYTED, Maracaibo, Venezuela, 1998.

[2] Manual of Rehabilitation of Concrete Structures, in: P. Helene and, F. Pereira (Eds.), Reinforcement and Protection, first ed, CYTED, Sao Paulo, Brazil, 2003.

[3] O. Troconis de Rincón and DURACON Collaborators, Effect of the marine environment on reinforced concrete durability in Iberoamerican countries: DURACON project/CYTED, Corrosion Science, v. 49, pp. 2832-2843, 2007.

[4] O. Troconis de Rincón, DURACON Collaborators, Concrete Carbonation in Ibero-American Countries DURACON Project: Six-year Evaluation, Corrosion V.71 (No.4) (2015) 546–555.

[5] O. Troconis de Rincón, DURACON Collaborators, Reinforced Concrete Durability in Marine Environments DURACON Project: Long-Term Exposure, Corrosion V.72 (No.6) (2016) 824–833.

[6] S. Mindess, J.F. Young, and D. Darwin, Concrete, 2nd ed., Prentice Hall, Pearson Education, Inc., Upper Sadle River, NJ, 07458, USA, 2003.

[7] C. Andrade Manual de Inspección de obras dañadas por corrosión de varillas, España, ACOR, Anes Gráficas, S. A., septiembre, 1988 (In Spanish).

[8] A.A. Torres-Acosta, A.A. Sagüés, Concrete Cracking by localized Steel Corrosion – Geometric Effects, Acids Mater. J. V. 101 (No. 6) (2004) 501–507.

[9] A.A. Torres-Acosta, M. Martínez-Madrid, Residual Life of Corroding Reinforced Concrete Structures in Marine Environment (July-August), J. Mater. Civ. Eng. vol. 15 (4) (2003) 344–353.

[10] E.I. Moreno, Carbonation of Blended Cements, Ph.D. Dissertation, University of South Florida, Tampa, Florida, USA, December, 1999.

[11] A. Majlesia, K. Khodadadi Koodiania, O. Troconis de Rincon, A. Montoya, V. Millano, A.A. Torres-Acosta, B. Rincon Troconis, Artificial neural network model to estimate the long-term carbonation depth of concrete exposed to natural environments (September), J. Build. Eng. V.74 (2023), https://doi.org/10.1016/j.jobe.2023.106545.

[12] NMX-C-414-ONNCCE-2017 “Industria de la Construcción - Cementantes Hidráulicos - Especificaciones y Métodos de Ensayo,” Organismo Nacional de Normalización y Certificación de la Construcción y Edificación, S.C., Ceres 7, Crédito Constructor, Benito Juárez, CP 03940, Ciudad de México, México.

[13] ASTM C136. Standard Test Method for Sieve Analysis of Fine and Coarse Aggregates, American Standard for Testing Materials International, 100 Barr Harbor Drive, PO Box C700, West Conshohocken, PA, 19428-2959 USA, 2006.

[14] ASTM C-39. Standard Test Method for Compressive Strength of Cylindrical Concrete Specimens. American Standard for Testing Materials International, 100 Barr Harbor Drive, PO Box C700, West Conshohocken, PA, 19428-2959 USA, 2021.

[15] ASTM C-496. Standard Test Method for Splitting Tensile Strength of Cylindrical Concrete Specimens, American Standard for Testing Materials International, 100 Barr Harbor Drive, PO Box C700, West Conshohocken, PA, 19428-2959 USA, 2017.

[16] ASTM C-469. Standard Test Method for Static Modulus of Elasticity and Poisson’s Ratio of Concrete in Compression, American Standard for Testing Materials International, 100 Barr Harbor Drive, PO Box C700, West Conshohocken, PA, 19428-2959 USA, 2022.

[17] ASTM C-642. Standard Test Method for Density, Absorption, and Voids in Hardened Concrete, American Standard for Testing Materials International, 100 Barr Harbor Drive, PO Box C700, West Conshohocken, PA, 19428-2959 USA, 2021.

[18] G. Fagerlund, Methods of characterization of pore structure, in 3 contributions to RILEM Committee pore structure and properties of materials, Report 41, Lund, Sweden, 1973.

[19] ASTM C-1876. Standard Test Method for Bulk Electrical Resistivity or Bulk Conductivity of Concrete, American Standard for Testing Materials International, 100 Barr Harbor Drive, PO Box C700, West Conshohocken, PA, 19428-2959 USA, 2019.

[20] ASTM C876. Standard Test Method for Half-Cell Potentials of Uncoated Reinforcing Steel in Concrete, American Standard for Testing Materials International, 100 Barr Harbor Drive, PO Box C700, West Conshohocken, PA, 19428-2959 USA, 1999.

[21] U. Angst, F. Moro, M. Geiker, S. Kessler, H. Beushausen, C. Andrade, J. Lahdensivu, A. Koloio, K. Imamoto, Sv Greve-Dierfeld, M. SerdarRILEM Tech 5 Lett , 2020, , 85–100.

[22] L.J. Parrott, A Review of Carbonation in Reinforced Concrete, Building Research Establishment, Department of the Environment, Garston, Watford, United Kingdom, 1987.

[23] S.O. Ekolu, A review on effects of curing, sheltering, and CO_2 concentration upon natural carbonation of concrete, Constr. Build. Mater. 127 (2016) 306–320.

[24] M. Otieno, J. Ikotun, Y. Ballim, Experimental investigations on the effect of concrete quality, exposure conditions and duration of initial moist curing on carbonation rate in concretes exposed to urban, inland environment, Constr. Build. Mater. 246 (2020) 118443.

[25] H.K. Wierig. Longtime studies on the carbonation of concrete under normal outdoor exposure, Proc., RILEM Seminar on the Durability of Concrete Structures under Normal Outdoor Exposure, Institut für Baustoffkunde und Materialprüfung der Universität, Hannover, (1984), pp. 239–249.

[26] E.E. Maldonado-Bandala, D. Nieves-Mendoza, J.L. Vela-Jimenez, P. Castro-Borges, Evaluation of pathological problems associated with carbonation and sulfates in a concrete tower with more than 50 years in service, Rev. ALCONPAT Int. Vol.8 (Issue 1) (2018) 94–107, https://doi.org/10.21041/ra.v8i1.284.

[27] R. López Celis, J.T. Pérez Quiroz, A.A. Torres Acosta, M. Martínez Madrid, W. Martínez Molina, L.E.Ariza Aguilar, E. Zamudio Cíntora, J. Genescá Llongueras, B. Valdez Salas, Durability of concrete exposed to different urban environments in Mexico, Technical Publication No. 292, Instituto Mexicano del Transporte, Sanfandila, Queretaro, Mexico, 2006 (In Spanish).

[28] A. Torres Acosta, J.T. Pérez Quiroz, P.Castro Borges, C. Andrade, N. Rebolledo Ramos, F.Almeraya Calderón, C. Gaona Tiburcio, E.I. Moreno, T. Pérez López, M. Sosa Bas, M. Martínez Madrid, W. Martínez Molina, E. Alonso Guzmán. “Concrete carbonation in urban and urban/marine environments in Mexico and Spain,” 3rd National Congress ALCONPAT 2008, Chihuahua; Chihuahua, Mexico, 12-14 November, 2008. (In Spanish).

[29] A.A. Torres-Acosta, A.A., P.Y. González-Calderón. “Opuntia Ficus Indica (OFI) mucilage as corrosion inhibitor of steel in CO2-contaminated mortar,” Materials MDPI, Special Issue "New Findings of Portland Cementitious Materials," Vol. 14, Issue 5, (2021) 1316, https://doi.org/10.3390/ma14051316.

[30] A.A. Torres-Acosta, Considerations to avoid corrosion rate estimate error of the reinforcing steel if based only on concrete’s electrical resistivity, Corrosion Vol. 80 (Issue 4) (April 2024), https://doi.org/10.5006/4482.